Aalto University
School of Engineering

Aisha Ambreen

Computational modeling of flow-induced alignment of nano-cellulose fibrils

Master's Thesis submitted for approval for the degree of
Master of Science in Technology
Aalto University, Finland

Espoo, Date: 29.05.2017
Supervisor: Asst. Prof. Jarkko Niiranen
Advisor(s): Asst. Prof. Jarkko Niiranen

Acknowledgment

I am grateful to my supervisor Asst. Prof. Jarkko Niiranen for his support, understanding and kindness throughout this project. I enjoyed my time working with him.

I would also like to thank Dr. Djebar Baroudi for not only using his precious time to review this work and his valuable comments on this project but also for his continuous support throughout my studies. A special thanks to Ms. Meri Lundahl and Mr. Pezhman Mohammadi for providing me detailed information essential for this research.

I am grateful to Academy of Finland for funding my thesis (decision number 273609). My experience in research was productive and rewarding. I am also indebted to Government of Finland for providing me an opportunity to affordable world class education.

Finally, I would like to express my gratitude towards my classmates, teachers and the university staff for making my education experience exciting and memorable.

Author

Aalto University
School of Engineering

Aalto University, P.O. BOX 11000, 00076 AALTO
www.aalto.fi

Abstract of master's thesis

Author Aisha Ambreen

Title of thesis Computational modeling of flow-induced alignment of nano-cellulose fibrils

Degree programme Master in Structural Engineering

Major/minor Structural Engineering **Code** Eng3039

Thesis supervisor Assistant Professor Jarkko Niiranen

Thesis advisor(s) Assistant Professor Jarkko Niiranen

Date 29.05.2017 **Number of pages** 58+10 **Language** English

Abstract

Long continuous cellulose fibers are synthesized from cellulose nanofibrils (CNF) by using wet and dry spinning techniques. The quality of cellulose fibers will depend on several properties such as plant source, aspect ratio and alignment of cellulose nanofibrils. Nanofibrils are aligned during the flow in a capillary tube while spinning. Variation of flow parameters and geometry of the capillary tube can change the alignment of fibrils.

In the present work, flow fields inside the capillary tube were generated by simulating the suspension by using a commercial finite element software and the parameters were changed systematically to observe their effect on the flow profiles and to co-relate the results with experimental studies conducted in Aalto University. Parameters selected for the present work were flow rate, concentration of CNF suspension, diameter and length of the capillary tube. Carreau model was used to predict the non-Newtonian behavior of CNF suspensions and its parameters were obtained by plot-fitting the rheological data.

The work met with certain complexity due to highly non-linear behavior of the Carreau model with parameters fitted for rheological data of CNF suspensions. However, some important conclusions have been obtained from the results. It has been shown that the main parameter which affects the alignment of fibrils inside the flow is shear rate. Decreasing diameter and increasing flow rate both have resulted in increase in shear rate throughout the diameter of the capillary tube. Simulation of CNF suspensions with different concentrations resulted in an unexpected trend for velocity profiles and change in length of capillary did not affect velocity profiles or shear rate inside the capillary tube. The effect of these parameters was also studied for shear stress and it was shown that the change in diameter, flow rate and concentration of suspensions significantly change the trend of shear stress profiles.

Keywords Cellulose nanofibrils, non-Newtonian fluid, simulation

Contents

1 INTRODUCTION

1.1 FIBERS

Fibers are synthetically manufactured or naturally available substances with very high aspect ratio, often used to make other materials or used as a reinforcement in composites. Fibers have also wide applications in textile, papers and furniture because of their high strength and durability. Naturally available fibers are cotton, linen, silk and wool etc., whereas synthetic fibers are produced using a mechanism such as polymerization of petrochemicals. Examples of such manmade fibers are polyester and nylon and the synthetically made cellulose fibers (also known as regenerated fibers) created from dissolving cellulose in chemicals include viscose, rayon and lyocell.

With the passage of time, realization of positive effects from the use of environmental friendly products has shifted the trend from plastic fibers to the fibers produced from natural sources. The CIRFS 2005 report showed that the use of manmade fibers has been increased to 70% worldwide and this percentage is even higher in Europe. With the advancements in medical sciences, world population has increased exponentially in past few centuries which has resulted into more occupation of land primarily due to higher food cultivation and urbanization. As a consequence, agricultural land available for the production of cotton as the main source for natural fibers has reduced. It is not feasible to meet all the requirements only by using natural fibers due to high demand of fibers for textile and paper industries for ever size growing of population,

On the other hand, synthesis of manmade fibers involves the use of toxic chemicals which is seen as a biggest disadvantage of these fibers. For example, for the production of regenerated cellulose based fibers (such as rayon), carbon disulphide is used which is proven to be very hazardous for the environment and health. Although production of manmade cellulose fibers requires use of some chemicals but yet it is more environmental friendly than plastic synthesized fibers because they are abundant, biodegradable and renewable materials. Besides, more research is being carried out on how to improve the methods of manufacturing cellulose fibers without using any harmful chemicals. [1]

1.2 INTRODUCTION TO CELLULOSE NANOFIBRILS

National Science Foundation has declared fibers with 100 nm or less are identified as nanofibrils, produced by splitting of bio component fibers. Nanofibrils are used in medicine, artificial organs, tissue engineering and other medical applications [2]. Uses of the nanofibers in the textile industry for production of shoes, sport dresses and diapers of kids is also very common.

Cellulose nanofibers (CNFs) are a class of renewable and biodegradable natural reinforcement materials gaining popularity because they are readily available, ecofriendly and possess good mechanical properties. In plants, cellulose forms the structural component of cell wall providing rigidity and strength. It consists of bundles of fibers which are 10-20 nm in diameter and several micrometers in length consisting of polysaccharide chains (β-D-glucopyranose units linked together by β-1-4-linkages) that are packed to nanofibers and plays a hierarchical role in providing stiffness to the tree, as shown in ***Figure 1***.

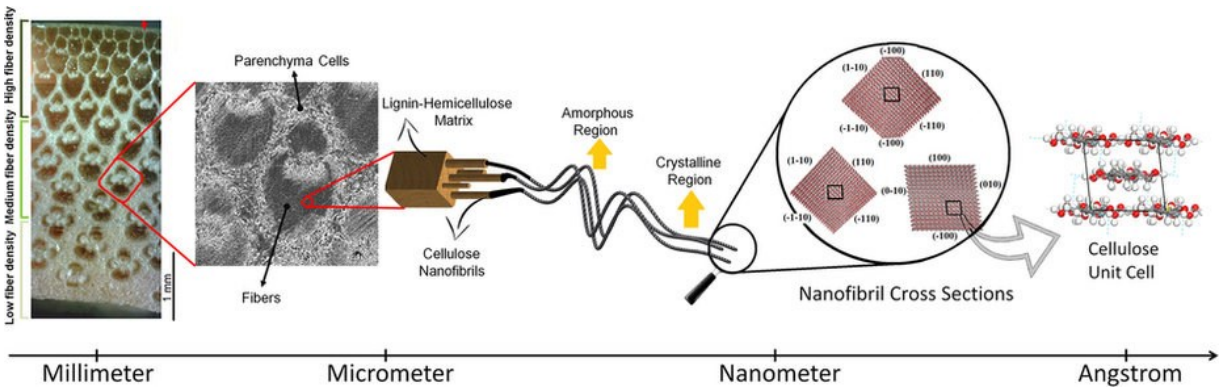

Figure 1: *Hierarchical structure of bamboo fibers at different scales down to unit cells [3].*

CNFs are made from any cellulose containing material which is usually wood pulp, obtained by a mechanism which involves the removal of lignin from the original wood fibers. By using high shear forces and sometimes adding chemicals rip apart wood fibrils and their crystalline parts into nanofibers. Another process of making nanoscale fibers involves the use of Acetobacter xylimum bacteria and the result is nanostructured whiskers [4]. Not only manufacturing process of CNFs

requires less use of dangerous chemicals, raw material for it can be obtained in huge quantities by careful forestation using the former method thus developing a greener process and unlike many other reinforcements, CNFs are totally degradable.

1.3 APPLICATION OF CELLULOSE FIBERS

Currently, most of the composites are made from reinforcements which are produced by using dangerous chemical solvents whose disposal and production is rather difficult and recycling of such conventional composites is also not an easy task due to their non-degradability. On contrary, CNFs when combined with degradable matrix such as poly lactic acid can result into a strong yet completely degradable composite.

CNFs also find a wide variety of other applications such as in paper, medical, pharmaceuticals, absorbents and textile industry. Their mechanical properties, with few exceptions, have been found to be of the same magnitude as of glass and Kevlar fibers in few cases [5], [6]. Mechanical properties of a composite can be improved with the dispersibility and functionalization of the cellulose nanofibrils (CNF) in the matrix but to achieve the mechanical strength of individual fibers to the same level yet needs to be explored. The reason why fibrils loose their crystallinity, and strength in first place, is that the manufacturing process usually breaks the bonds that tightly pack the bundles together.

1.3.1 Cellulose fiber-reinforced concrete

Cellulose fibers-reinforced concrete is rapidly growing technology in construction industry for the development of the durability of cement-based composites. An extraordinary combination of mechanical and physical properties and their environmental benefits has been a driving force behind their use as alternatives for synthetic fibers. The reinforcements based on cellulose fibers can be divided into two types, (1) short fibers randomly distributed in the mortar matrix and (2) aligned reinforcement. In the former technique, mortar matrix is made by preparing the slurry by adding matrix materials in water which has short fibers dispersed inside it and then later water is removed from slurry by using vacuum dewatering technique [7], [8]. In the latter reinforcement type, the reinforcement capacity is increased by using longer strands aligned. In one of the studies,

high performance cement-cellulose composites are reported to be prepared by using longer fibers [9]. Cellulose fiber reinforced Iron blast furnace slag exhibited improved flexural strength and other mechanical properties when compared with ordinary Portland cement mortar [10]. Another study was conducted to explore the effect of cellulose fibers on cement mortar and concrete [11]. The fibers were shown to have little impact on the flexural strength but they enhanced the stiffness of the matrix with an increase in the fibril content, which means that only a limited amount of fibers can be used. However, cellulose fibers had a remarkable effect on the shrinkage control of the cast materials. In the same study, fibers with different coatings were used but there was no effect of the coating on the reinforcement. Similarly, adding some plasticizers in the concrete did not show any difference in the performance of reinforcements.

1.3.2 Cellulose-reinforced ice structures

Ice structures are known to be very brittle, weak and show extremely high creep compared to conventional concrete structures. In construction industry, ice composites have also been reinforced by wood pulp known as pykretes [12].

1.4 MECHANICAL PROPERTIES OF CNF

Natural fibers are composed of cellulose, hemicellulose, lignin and pectin and variation in the percentages of these components defines the mechanical properties of the fibers. Hemicellulose absorbs the moisture; lignin is responsible for the thermal stability and it is cellulose which adds strength and stiffness in the fibers due to the strong hydrogen bonds [13].

Cellulose nanofibers have a huge advantage to be used as reinforcement in composites because of the high mechanical properties (elastic modulus and tensile strength) combined with its light weight. Specific strength of the cellulose presented by Al-Hosseiny can be seen in comparison with the other strong metals such as Aluminum and Steel [14]. In ***Figure 2***, red dots show the fibers obtained from different parts of the tree, Cellulose Ⅰ represents the natural fiber and Cellulose Ⅱ is the regenerated fibers when crystalline structure of polymer chains in Cellulose Ⅰ is altered permanently by sodium hydroxide treatment. The natural cellulose is 50% stiffer than the Cellulose

II [15], which suggests that there is still room for an improvement in the stiffness of manmade fibers.

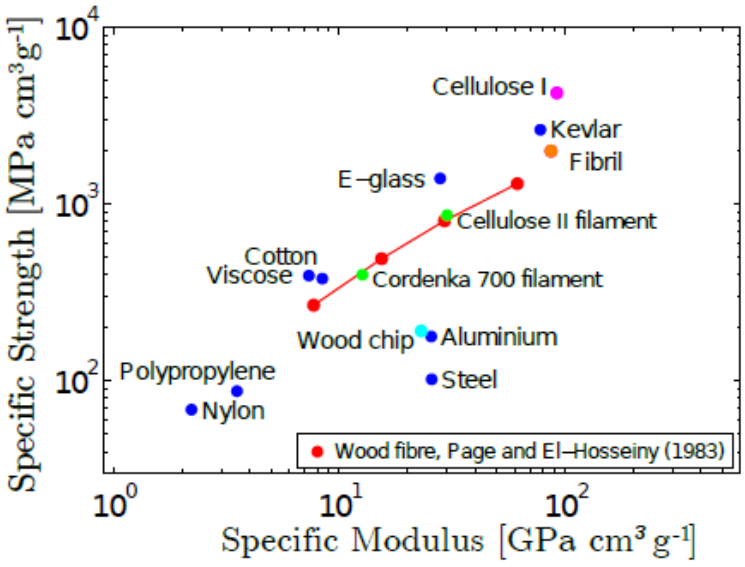

Figure 2: *Specific strength for different materials given against their specific Young's moduli.*

1.5 SCOPE OF THE THESIS

The fibers that have been produced up until now have lower strength as compared to the single natural fibril. This implies that there are some factors which, are affecting the strength of these fibers while they are being synthesized. It was observed that stiffness of various parts of tree varies depending on the orientation of fibrils along the axis of a fiber and this led to a research on improving the orientation of nanofibrils to produce stronger fibers. Fibers are synthesized by using a variety of spinning techniques which involve various steps starting from the preparation of the nanocellulose suspension to the drying of spun fibers. The step which plays key role in aligning fibrils during this process is when suspension is allowed to flow through a spinneret or capillary tube. Naturally different flow conditions during spinning improve or hinder the alignment of fibrils during the flow. A biomimetic spinning approach including various flow parameters i.e. flow rate,

suspension concentration, length and diameter of capillary tube has been investigated by systematically changing these parameters [16].

This master thesis is devised to numerically study the effect of those parameters on the flow behavior of the suspension and to better understand the relation between the flow profiles and orientation of the fibers. Computer can be an efficient tool to visualize the situation which are impossible to observe in real life experiments and to make changes easily in the pipe geometry or the material properties.

The scope of this work is to investigate thoroughly the flow properties of cellulose nanofibrils suspension inside an experimental setup and to validate the conclusions derived from experiments performed in the laboratory. The purpose of this research is also to use a commercial software to study the flow fields and to observe to what extent such a software can be exploited research purposes in especially for fluids with complex rheology.

2 LITERATURE REVIEW ON CELLULOSE NANOFIBERS

2.1 PREPARATION OF CELLULOSE SUSPENSIONS

Cellulose nanofibrils suspension can be prepared by using a variety of sources ranging from micro-organisms [17] to soft wood [18]-[20] and hard wood [21], [22], new and regenerated fiber sources [23] with using different treatments and spinning methods with slight variations in the geometrical setup. A very general method is mentioned here step by step in detail in order to introduce reader the various steps cellulose fibrils go through from their extraction to the spinning of fibers. Each step plays a unique role to favor or hinder the alignment of nanofibrils during the flow of the suspension.

2.1.1 Separation of cellulose from the wood

Cellulose nanofibrils can be obtained from different cellulosic sources but most commonly they are separated from wood pulp. Non-wood sources like palm trees [24], sugar beet [25], wheat straws and soy hulls [26] are rich in cellulose and have also been successfully used to extract CNFs. While preparing CNFs from wood, Cellulose must be separated from the other components present in wood like lignin by either dissolving or degrading it when the chemical pulping is carried out [27]. Kraft pulping is the most extensively used method which involves the dissolving of wood pieces in a mixture of hot water and sodium hydroxide and sodium sulfide [28] and later the pulp is bleached to brighten its color.

2.1.2 Mechanical Treatment

When the pulp is ready, the nanofibrils are fibrillated in the sample by using different mechanical treatments. Cellulose pulp is pre-treated to weaken the intramolecular hydrogen bonds, which helps in avoiding the high consumption of energy during the mechanical treatment. The three most common devices used for the fibrillation of cellulose are micro-fluidizer, Gaulin Homogenizer and a grinder device developed by Masuko (Tokyo, Japan) [30]. The first two devices are based on the system where the pulp or slurry is injected with high pressure between the pistons or in the

fibrillation chamber and grind devices crush the cell wall by applying high shear forces with the help of two grinding stones [30].

Cellulose slurry can also be treated by action of different enzymes. In the enzymatic treatment, a nature friendly enzyme named as cellulase (endoglucanase or cellobiohydrolases) is used to weaken the interaction between microfibrils which later on facilitates the disintegration of fibrils during the mechanical treatment [29]. The hydrogel obtained at the end is centrifuged to remove very short fibers from the mixture and it can be further diluted with deionized water to produce suspensions with different amount of solid content.

2.1.3 Pre-treatment of the cellulose fibrils

Cellulose fibrils have been used unmodified for spinning of fibers but some of the studies have carried out a pre-treatment of fibrils to enhance their properties [15], [21]. The pre-treatment of the cellulose sample is carried out by TEMPO-oxidation of non-refined never-dried bleached fibers using an alkaline system [31]. TEMPO-oxidation is the oxidation of cellulose fibers at pH 10–11 in the presence of a catalyst 2,2,6,6 tetramethyl-1-piperidinyloxy (TEMPO) and NaBr at room temperature. This results in the formation of carbohydroxyl groups providing a negative charge which helps in the dispersion of the fibrils by overcoming the hydrogen bonds binding them together. The fibrils can also be dispersed by treating them mechanically with a blending device, i.e., Waring-Blendor12.

2.1.4 Stability of CNF suspension

Cellulose nanofibers are not soluble but are highly dispersible in water. Stability of the solution means that solution does not undergo any changes in the rheological parameters at given conditions. Gelling in fluids is defined as the solidification or increase in viscosity until the fluid molecules make a network which restricts its flow. Gelation can occur with or without disturbing the surrounding conditions or it can be induced by changing the temperature or adding a chemical agent. The thickening of the gel is affected by the molecular structure and concentration as well as the pH, number of ions and the temperature of the system [32]. Gel formation on the early stages of the fiber spinning process could adversely affect the flow of suspension and hindering the

continuity of the process. In CNF suspensions, gel can be formed at elevated temperature due to the alkaline nature of the suspension. The gelation effect has also been observed to rise with the increase in concentration of fibers [33].

2.2 RHEOLOGY OF CNF SUSPENSIONS

Cellulose suspensions exhibit an intense shear thinning and thixotropic behavior and the fineness of fibers affect the viscosity of the suspension. Generally, the finer the fibrils, the higher is the viscosity provided that the solid content concentration is kept constant. The thixotropic behavior of CNF suspensions also depends on the treatment of nanofibrils. Viscosity was reported to increase when the treatment time for the nanofibrils was increased for a given concentration as shown in ***Figure 3*** [34]. In the same study, suspensions demonstrated a linear increase in the viscosity with the increase in concentration, and after a critical limit the viscosity follows the power law [34].

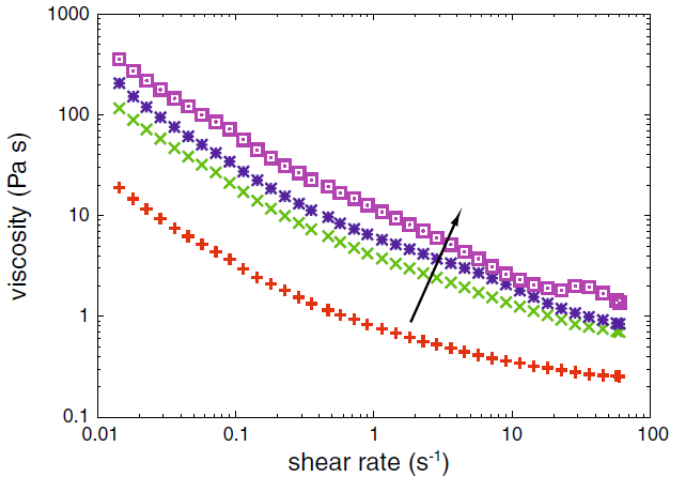

Figure 3: *Viscosity of oxidized cellulose suspension with 0.4% concentration corresponding to shear rate. The arrow shows the increase in the treatment time [34].*

2.2.1 Rheometer

Rheometer is a device used to measure the apparent viscosity of non-Newtonian liquids or suspensions under applied forces. There are different kind of rheometers like dynamic shear rheometer, linear and rotating rheometers. Plate-plate and vane geometries are mostly used for the characterization of CNF suspensions. A vane rheometer has a propeller which rotates inside a cylindrical geometry to avoid boundary slip.

2.2.2 Suspension viscosity model

A suspension is a heterogeneous mixture of solute and solvent in which solute particles are suspended in the solvent medium. One model which was used recently for cellulose suspensions is given as follows [35].

It is because of the thixotropic behavior (time-dependent rheology) of the CNF suspensions researchers have proposed models which takes into account the evolution of rheological behavior in time. One such model was developed by using a methodology which combines the Population Balance Equations with an equation of state to calculate the suspension viscosity taking into account the anisotropy of the particles. The population balance equation proposed by Smoluchowski [36] is given as

$$\frac{dn_i}{dt} = \frac{1}{2}\sum_{j=1}^{i-1} k^{(a)}(1-j,j)n_{i-j}n_j - \sum_{j=1}^{\infty} k^{(a)}(i,j)n_i n_j - k^{(b)}(i)n_i + \sum_{j=i+1}^{\infty} \beta(i,j)k^{(b)}(j)n_j \qquad (1)$$

where *i, j* denote the number of monomers belong to different size classes, and *β(i,j)* is the fragment distribution function. $k^{(a)}$ and $k^{(b)}$ are aggregation and fragmentation kernels which are functions of laminar flow as given below

$$k^{(a)}(i,j) = c_e \frac{4}{3}\dot{\gamma}(r_i + r_j)^3$$

$$k^{(b)}(i) = \dot{\gamma} e^{\left(-\frac{2F_c}{5\pi r_i^2 \mu \dot{\gamma}}\right)},$$

where c_e is a collision efficiency factor because of the porosity, inter-particle potentials, and hydrodynamics of the fractal aggregates in the first equation [37] and F_c takes into consideration the cohesive forces between aggregates and r_i is the radii of the aggregate. The viscosity of the suspension is represented according to the Krieger type expression.

$$\mu = \mu_0 \left(1 - \frac{\varphi_{eff}}{\varphi_m}\right)^{-k}, \tag{2}$$

In this expression, μ_0 is the dynamic viscosity of the pure fluid, k is a constant dependent on the concentration of suspension, φ_{eff} is the solid-phase volume fraction and φ_m is the maximum packing concentration.

2.3 SPINNING TECHNIQUES OF FIBERS

A variety of spinning techniques is used to produce a continuous fiber of indefinite length. Typically, polymer process techniques involve extrusion of fibers either through melt-spinning or solvent-spinning. The high hydrophilicity or water affinity of cellulose and absence of melting stages for cellulose fibrils drop out the possibility of melt-spinning. Solvent-based spinning methods are further divided into wet-spinning, dry spinning and dry jet spinning. Each of these techniques requires dissolved polymers or nanofibrils in a solvent and then the spun fibers are extruded through a flow generating equipment, i.e., pump syringes, extruders, capillary tubes or even 3D-printers [38].

2.3.1 Wet Spinning

In the wet spinning process (***Figure 4***), the cellulose dope is pumped through a capillary tube or a spinneret at a known flow rate and it is extruded from the other end into a coagulation bath. The solution in the bath immediately coagulates the CNF dope. Coagulation is a process in which dope forms a gel-like structure and is separated from its solvent due to the formation of a membrane between solvent and non-solvent in the coagulation bath. This separation membrane helps their mutual diffusion [1]. After few minutes, the fibers are dried in the air and collected in the

continuous form. The fibers must be kept stretched by fixing their ends to prevent the fibers from contraction which has been observed during the cellulosic paper formation [39].

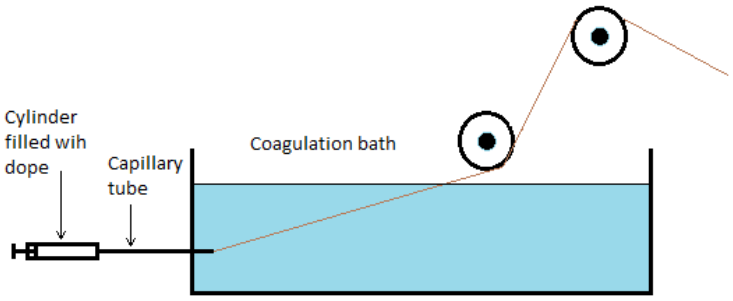

Figure 4: *Schematic diagram of wet spinning process.*

2.3.2 Dry Spinning

The polymers dissolved in the solvent are extruded through a spinneret in the dry spinning of fibers. When the dope is emerged out from the other end, hot air is blown on the dope, which dries out the solvent. Since the fibers are directly extruded in the air or an inert gas, this process of making fibers is known as dry spinning.

2.4 CHARACTERIZATION OF MATERIALS

Materials fabricated in the laboratory are thoroughly investigated to obtain information about their structure and composition. Different techniques are available to investigate the structure and properties depending on the material nature, some techniques yield qualitative information such as surface images and others give quantitative information like concentration of atoms in the sample. Technology advancements have enabled even two or three-dimensional images of solids.

2.4.1 Optical Microscope

An optical microscope is consisted of lenses to magnify the images of samples placed underneath them. Optical microscopes usually use visible light to illuminate the sample. Polarized light

microscopy is referred to an optical microscopy technique which uses polarized light for illumination. This technique is more suitable for birefringent samples as polarized light has strong interaction with such samples producing images in a contrast with the background.

2.4.2 Electron Microscope

Remarkable revolution in nanotechnology has made it possible to characterize the nanomaterials revealing the morphology of a specimen to a great extent. The basic principle of the electron microscope technique is very similar to optical microscopy. Electron microscopes replace light with high energy electrons for illumination and utilize electromagnetic instead of ordinary lenses for magnification when compared to optical microscopes. There are two types of instruments used for electron imaging: TEM (transmission electron microscope) and SEM (scanning electron microscope).

In TEM, the transmission mode measures the intensity produced as a result of the electron source hitting a transparent sample. Conversely, SEM features the scanning of a focused electron beam over selected regions of an opaque sample. The electrons interact with atoms in the sample, producing various signals that not only explore surface topography but also reveals in-depth information about the morphology and composition of the specimen. The information retrieved is based on the penetration of electrons in the specimen, which in turn depends on the energy of electrons. Electron energy can be varied by increasing or reducing the applied voltage.

2.4.3 X-ray Scattering

When electromagnetic radiation of certain length is passed through a structure with high wavelengths as compared to the incident wavelength, it results in deflection of the wave at some angle. If the angle is very small ($0\text{-}10^0$), then this technique is known as Small Angle Scattering (SAS) and if this technique uses X-rays, then it is called Small Angle X-Ray Scattering (SAXS). If the angle is large ($10\text{-}90^0$), the technique is referred as Wide Angle X-Ray Scattering (WAXS). These techniques are mostly used to observe the morphology of crystalline, semi-crystalline or amorphous structures. The underline principle of these techniques is very simple as presented in ***Figure 5***, a beam of X-ray is allowed to pass through a sample and intensity of scattering of waves

is recorded on a plate detector located on the other side of the sample. This technique is widely used to observe the alignment of fibrils during the flow or in the final fiber, and the orientation parameter is dependent on the intensity of light passing through the sample.

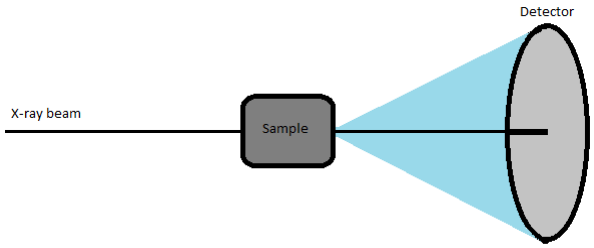

Figure 5: *Schematic diagram for x-ray scattering.*

2.5 ALIGNMENT OF NANOFIBERS

The filament properties and morphology are influenced by many factors. As it has been already discussed that the fibrils go through several stages during manufacturing, i.e., extraction from wood source, pre-treatments, dissolution and spinning etc. All these processes contribute in the ultimate mechanical properties of the spun fibers. In this section, it will be discovered how the alignment of fibrils affect the final morphology of a fiber. Alignment of fibers can easily be achieved easily in a flow since the flow has a natural ability to align fibers in the direction of flow streamlines. Alignment of fibers through this process is a cheap technique and results into continuous fiber [40], [41].

The procedure of developing a structure by cellulose fibrils can be demonstrated by a simple example of paper composition. Once the fibers are extracted from the wood, they are suspended in water and spread on a permeable sheet which, allows the fibers to be filtered out from water and form a web like structure. Even at lower concentrations, fibrils are known to make flocs due to their high aspect ratio. To prevent this flocculation and to obtain a homogeneous structure, the suspension is allowed to go through an extensional flow which not only helps them to spread more evenly but also make them more aligned in the flow direction [42], [43].

Alignment of the fibrils in the direction of the flow can be achieved either by a shear induced laminar flow or a purely extensional flow. Jeffery was the first person to observe and predict that shear between fluid layers helps in the alignment of fibers in a laminar flow [44]. Alignment of the fibers in an extensional flow is verified through series of experiments performed by Mason [45]. Håkansson designed a process to create an extensional flow field which can control the fiber orientation distribution [46]. The difference between these two processes is that in the shear-induced flow there is no stable equilibrium orientation due to continuous rotation of fibrils but the orientation exists in the purely extensional flow.

2.4.4 Fibril orientation in an extensional flow

The process of developing an aligned structure for the end product consists of two steps, orienting the nanofibrils in one direction by a fluid flow and locking the aligned fibrils by creating a gel transition state.

The setup proposed in the dissertation by Håkansson, known as flow focusing device, comprises of three inlet channels and one outlet channel, illustrated in ***Figure 6***.

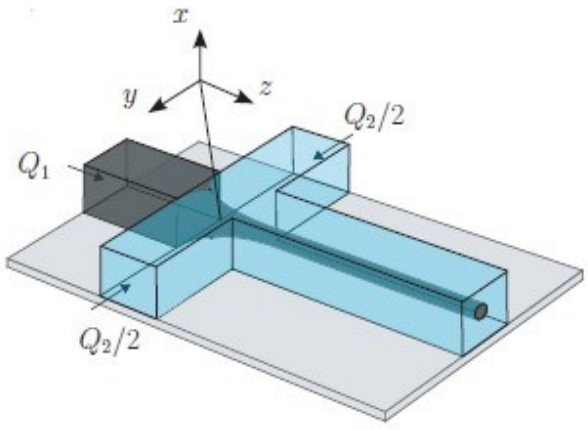

Figure 6: *Flow focusing channel designed by Håkansson [46]*

In this device, the core fluid is directed by two sheath flows from the side which results in an extensional flow. Shear inside the core flow is very small which prevents the constant flipping

motion of the fibrils. Two conditions are required for this process; (1) fibrils must be aligned before the gelation of particles, which in turn must happen before the fibrils lose their alignment due rotary motion caused by Brownian diffusion; and (2) the transition gel must occur before the liquid is discharged out of the channel. In this study, the orientation of the fibrils during the flow has been gathered by visualizing the alignment of fibrils through polarized light (POM) and Small Angle X-Ray Scattering (SAXS) setups. The sample is placed between two crossed polarized filters and the light is allowed to pass through these filters. When particles started aligning, the oriented bulk structure caused the suspension to be birefringent. Alignment of the fibers was simply estimated by the intensity of light, the more light passing through the second filter, the more aligned are the fibrils. An order parameter was introduced by Håkansson to quantify the orientation distribution from the variation of the intensity extracted from the scattering images. The order parameter was scaled to 0 and 1 for randomly and perfectly aligned fibrils, respectively, in the flow direction.

2.4.4.1 Numerical model for orientation

Håkansson uses a numerical model based on the Smoluchowski equation (1) for the evolution of the fibril alignment in terms of the orientation distribution along the centerline of the flow focusing device was presented. The orientation distribution $\Psi(r,p,t)$ is a function of position r, orientation p, time t and affected by two forces, the force from fluid and the rotary Brownian motion. The one dimensional Smoluchwoksi equation along the center line can be written as follows:

$$\omega^* \frac{\partial \Psi}{\partial z^*} = \frac{1}{\sin\phi} \frac{\partial}{\partial \phi} (\widehat{D}_r^* \sin\phi \frac{\partial \Psi}{\partial \phi} - \sin\phi \, \dot{\phi} \Psi) \qquad (3)$$

The superscript (*) in the above equation shows a non-dimensional quantity, ω is the velocity in z-direction, ϕ is the azimuthal angle, $\dot{\phi}$ denotes the angular velocity for axisymmetric flow which depends on the stretching of fluid and $\widehat{D}_r$ is the rotary diffusion constant. According to this model, alignment should increase with the increase in the extension rate. Evolution of the fibril orientation (predicted by Smoluchowski equation) inside the extensional flow can be seen in ***Figure 7***. As it is clear that first there is a sudden rise in the orientation but then the fibrils seem to lose their orientation after they have been entered in the extensional flow. Namely, as soon as the extensional

flow becomes constants, the effect of Brownian motion has overcome and the fibrils start losing their alignment. Moreover, Newtonian fluid with higher viscosity of 40 nMPa-s was also observed to work fine for the Smoluchowski equation to predict accurate orientation. In the same figure, the rotary diffusion constant is also varied by increasing its value and as one can expect it results in fibrils losing the orientation quickly.

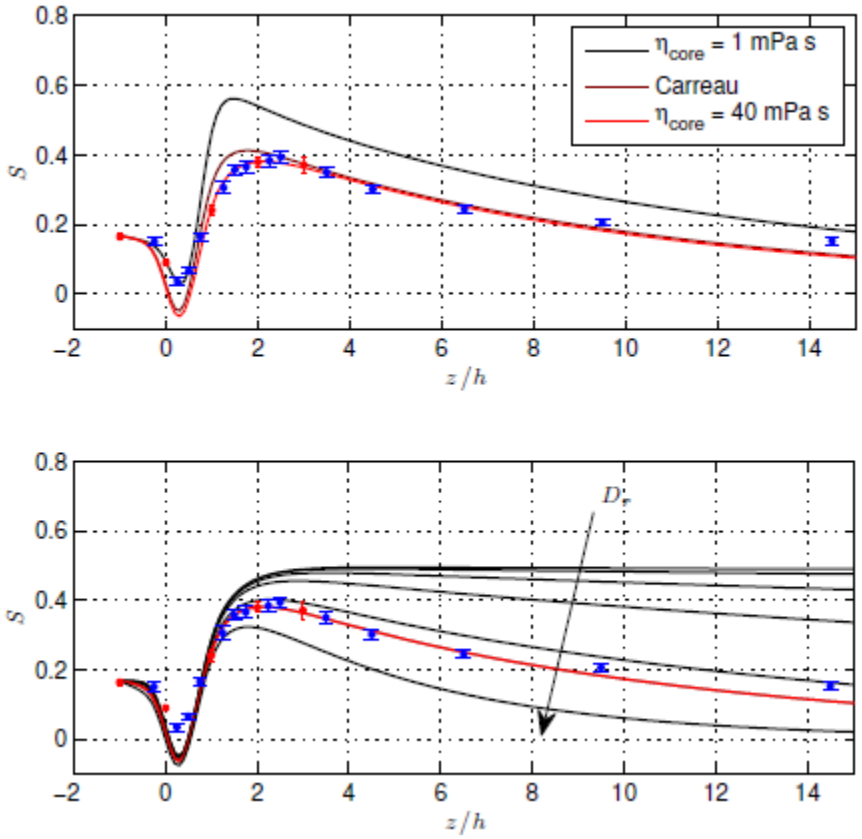

***Figure** 7: Measured and computed order parameter, the first plot area includes the comparison of different viscosity models and the second plot is an illustration for the variation of rotary diffusion parameter in the Smoluchowski equation. The red line corresponds to the best match with the experimental results [46].*

The numerical model provided for the orientation of the model overestimated the orientation while increasing the extension rate since when the experiment was conducted with the double extension

rate, it did not improve the alignment as predicted by the Smoluchowski equation as shown in ***Figure 8***. For the lower flow rate, orientation predicted by the numerical model (represented with solid lines) perfectly fits the orientation obtained from the experimental setup.

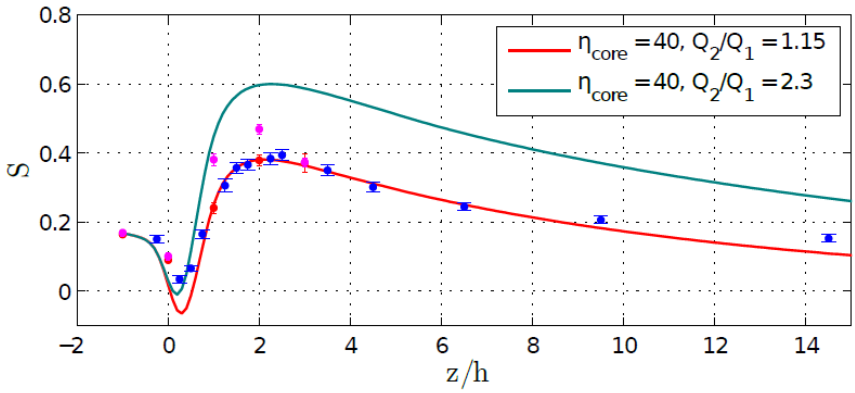

Figure 8: *Order parameter across the downstream positions of the channel with the increased flow rate; the dots are representing the experimental results, with pink dots for the doubled sheath flow [46].*

2.4.5 Alignment by shear flow

A theoretical study on the orientation of fibers in the shear flow presented by Jeffery [44] shows that most of the elongated particles keep themselves aligned to the plane of the flow and spend only a fraction of time rotating in the flow. This rotation occurs due to the mismatch in the velocity of the fiber and the velocity of the surrounding streamlines in the shear flow.

Shear-dependent alignment is shown in ***Figure 9***. This is a characteristic log-log graph for shear thinning non-Newtonian fluids between shear rate and apparent viscosity (explained in detail in the next chapter). The region with constant viscosity is called the Upper Newtonian Region and it does not help in the alignment of fibrils [65]. The linear part of the graph is the Shear Thinning Region where apparent viscosity is decreasing with the increase in the shear rate and this region aids in the alignment of fibers. Finally, the third region known as the Lower Newtonian Region has the maximum alignment where apparent viscosity is virtually zero. This region is not observed in most of the cases since it occurs with the degradation of molecules at very high shear rates [65].

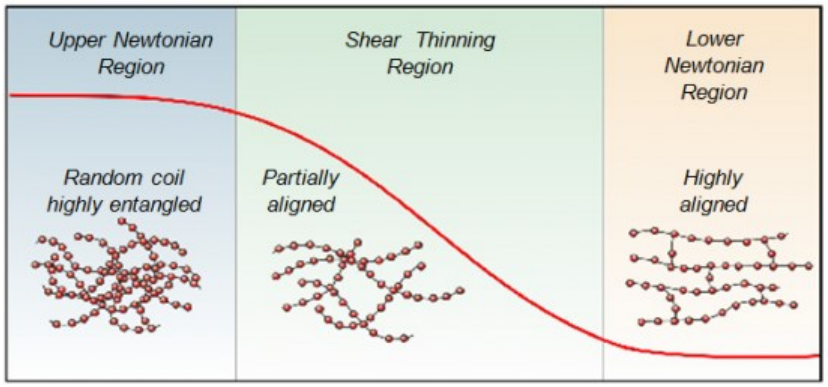

Figure 9: *Characteristic graph for shear thinning fluids [65].*

2.4.6 Effect of the alignment on the properties of Cellulose filaments

A significant amount of research has been performed to enhance the mechanical properties like impact toughness, tensile strength, Young's and shear moduli in a variety of polymeric composites by aligning the fibers [47]. Alignment has even a significant effect on the wear resistances in ceramics [48], [49]. It is quite clear that fiber alignment not only enhances the mechanical properties of the composites but also the isolated spun cellulose filaments produced as a result of increased nanofiber alignment along the fiber axis have better strength [15].

Cellulose nanofibrils can be used as nano-reinforcement for polymers [50] and nano-composites or as building blocks for new material since its stiffness is as high as Kevlar's [4]. A study conducted by Dingle [51] shows that the tensile strength and stiffness of the composites would be greater in the direction of fiber alignment as long as the fiber-matrix bond is strong enough to bear the load. This has been also confirmed by another study showing that aligned fibers were more effective than the randomly distributed fibers [52]. The main reason for this fact is the tensile strength of the aligned fibers. When a fiber tries to align itself in the direction of the flow, it experiences tension along its entire length, which improves its capacity to bear more stress and load [53]. A number of factors can have an effect on the alignment of fibers like the density of the fluid, fiber-fiber interactions, the length of the fibers and the flow rate. Furthermore, it has been suggested that the contraction of fibers while drying may result in the relaxation of oriented fibers [54].

2.4.6.1 Flow rate on alignment

Two methods for alignment of fibrils during the suspension of flow have been discussed so far: extensional flow and shear flow. In both cases, increasing flow rate means different thing. In the extensional flow, increase in flow rate increases the extension of the flow with almost zero or no shear rate but in the shear flow, it results in higher shear rates. Increasing the flow rate in the extensional flow does not further improve the alignment of fibrils during the flow as it has been discussed in Section 2.4.4.

In a laminar flow, shear forces generated from flow tend to align the cellulose nano-fibrils. These shear forces are directly proportional to the flow rate and can increase the alignment of fibrils during the flow and consequently can have a huge effect on the mechanical properties of the extruded fibers. Alignment of the tunicate fibrils in the flow direction are shown to improve with the flow rate increasing from 0.1 to 100 m/min [15]. This has been verified in another study where fibers were spun with two linear flow rates, 15 cm/s and 150 cm/s. Fibers spun with higher linear flow rate resulted in higher tensile strength and Young's modulus, and vice versa [16].

Although wood spun fibers at 100 m/min had Young's modulus of 23.6 GPa, tensile strength of 321 MPa, and elongation at break of 2.2%, fibers spun with flow rate more than 10 m/min were reported to have a hollow structure. It was argued that the hollow structure was resulted due to cylindrical coalescence of the tangentially assembled wood CNF based sheets [15].

An in-depth review, published recently on cellulose fibers, lists and discusses various parameters affecting the morphology, alignment and mechanical properties of fibers [55]. Young's modulus has shown to increase with the shear rate and the same trend has been reported for the tensile strength but after 200 s^{-1} of shear rate tensile strength started decreasing. Elongation break has also been reported to increase with the increase in flow rate. The author has calculated the shear rate for the experimental studies where one capillary tube with constant diameter throughout the length have been used and compiled the data from different studies to demonstrate the relation between the shear rate and mechanical properties of spun filaments. It is worthy to mention here that assuming shear rate constant in a spinneret is very unrealistic because of the complex rheology of CNF suspensions.

In all the studies mentioned above, increase in the flow rate has been shown to improve the mechanical properties of extruded fibers but it is problematic to report this as a general trend. Very high flow rates will shift the flow type from laminar to turbulent and eddies generated in the turbulent flow can disturb the alignment of fibrils. This has been confirmed by a study where the fibers were extruded from a flow with very high Reynold's number resulting in fibers of poor quality with Young's modulus of only 8.2 GPa and very low tensile strength of 118MPa [20]. In short, it can be concluded that the mechanical properties are improved when the alignment of fibrils improves and fibrils are primarily aligned because of the shear rate as long as the fluid is flowing smoothly like in case of laminar flow.

2.4.6.2 Fibril aspect ratio

In shear flow of fiber suspensions, there is a difference between the velocity field of the fluid which would exist in the absence of fibers and the velocity along the length of the fiber. This difference disturbs the environment of the flow which, in turn, causes the fiber to rotate. A fiber with a smaller diameter and higher aspect ratio will have small a difference in the aforementioned velocity fields, which will slow down the rotation of fibers keeping it aligned most of the time during flow [53].

There are no comparative studies carried out to see how changing the aspect ratio influences the orientations of cellulose fibers but there has been some research on determining the mechanical properties of CNF fibers obtained from different plants and trees. Cellulose extracted from different sources have different aspect ratio, for instance, CNF extracted from wood are of aspect ratio less than 200 mm [15]. Micro-organisms, algae and sea animal tunicate are other sources which have been used to obtain cellulose fibrils. One of the studies, using these sources reported obtaining micro fibrils with an aspect ratio greater than 500, after being treated by Tempo-oxidation [15]. This study has also reported higher tensile strength and Young's modulus than wood-based cellulose fibrils. Yet another study was carried out to see the difference in mechanical properties of softwood-based and hardwood-based CNF. Cellulose fibers taken from hardwood or angiosperm trees are shorter in length as compared to the ones taken from softwood origin. From these studies, we can hypothesize that besides the initial mechanical properties of fibers from different origins,

aspect ratio might have also played some role in the orientation of fibrils and improvement in the mechanical properties of spun fibers.

Tempo-oxidation improves the fibril aspect ratio and charge on the fiber. One study showed that the orientation of fibrils was improved for the TEMPO-oxidized CNF when compared with the orientation of unmodified CNF [55].

2.4.6.3 Fibril concentration

Fibers interact with each other during the flow depending on the concentration of suspension. In dilute suspensions, a fiber can rotate freely into aligned orientations but concentrated suspensions pose challenges for fibrils to align due to increased fiber-fiber interaction as reported in some of the studies [51], [56].

For unmodified CNF, most of the studies show that the mechanical properties of spun fibers can be enhanced by dilution of suspension until it reaches the limit where no more continuous fibers can be spun. CNF suspensions of minimum 1.36% and 3% solid contents have been used for spinning of continuous fibers for wet-spinning [16] and dry-spinning [22] respectively. On the other hand, concentration of fibers has an upper limit and it has been reported in many studies that increase in concentration up to certain extent leads to better mechanical properties. It has been observed in another experimental study carried out to see the effect of concentration on the orientation of fibers and their stiffness by using four concentrations ranging from 1.36-4 % w/v using identical conditions. CNF suspensions with concentration 2% and 3 % showed the highest values for Young's modulus and tensile strength [16]. A remarkable difference between the morphology of fibers along the axis of the fiber can be seen in the suspensions with different solid content concentration in ***Figure 10***. The overall difference in appearance can be clearly observed with CNF fibrils being more aligned throughout the sample in the CNF 2% sample than in the 4% sample.

In the CNF suspension, a non-Newtonian fluid, the velocity in the middle part of the flow profile is almost constant and the shear rate is very low. As a result, the suspension is expected to have

minimum or less alignment in the middle part of the capillary tubes, whereas near the walls fibrils must be highly aligned.

A microscopy study revealed that there was not much qualitative differences seen between the core of the fibers and the region around the surfaces and it was argued that the flow is not plug-like rather it is distributed (velocity is varying throughout the section).

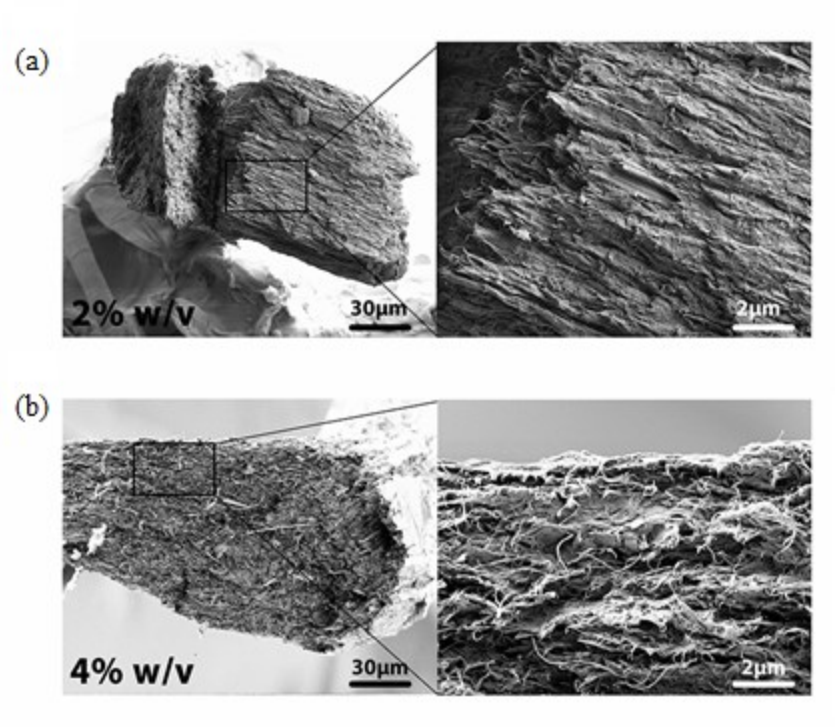

Figure 10: *SEM images and wide angle X-ray diffraction of a single fiber cross section. a) 2% w/v aq. CNF concentration using a flow rate of 150 cm/min in 1500 mm/0.5 mm capillary tube b) 4% w/v aq. CNF suspension extruded through 20 mm/0.75 mm capillary tube at a lower flow rate of 50 cm/min [16].*

Concentration of fibers in the suspension does not only affect the orientation of fibers due to fiber-fiber interactions but it also changes the behavior of the flow inside the spinneret or capillary tube. This change has been demonstrated by a series of experiments performed for suspensions with different concentrations, and velocity profiles were obtained by using magnetic flow imaging [57]. It is quite interesting that the velocity profiles and pressure drop at lower concentrations were similar to those of water, while with increased concentrations the velocity profiles shifted their trend to plug-shaped profiles (discussed in next chapter). The variation of flow rates for all concentrations revealed that the plug-shaped profiles for highly concentrated suspensions were not symmetric for lower flow rates due to the pronounced gravitational effects. Changes in the velocity profiles may also have an effect on the alignment of fibrils as it has already been discussed that fibrils align themselves due to the shear rate and this is why there is more alignment on the skin of spun fiber than in the core. More parabolic profiles mean that the fibrils can align themselves throughout the cross section of injections or capillary tubes.

3 BASICS OF FLUID MECHANICS

3.1 LAMINAR FLOW

In fluid dynamics, laminar flow, also known as streamline flow, occurs when a fluid flows in parallel layers, with no disruption between the layers. At low velocities, the fluid tends to flow without lateral mixing and adjacent layers slide past one another exerting shear force on each other.

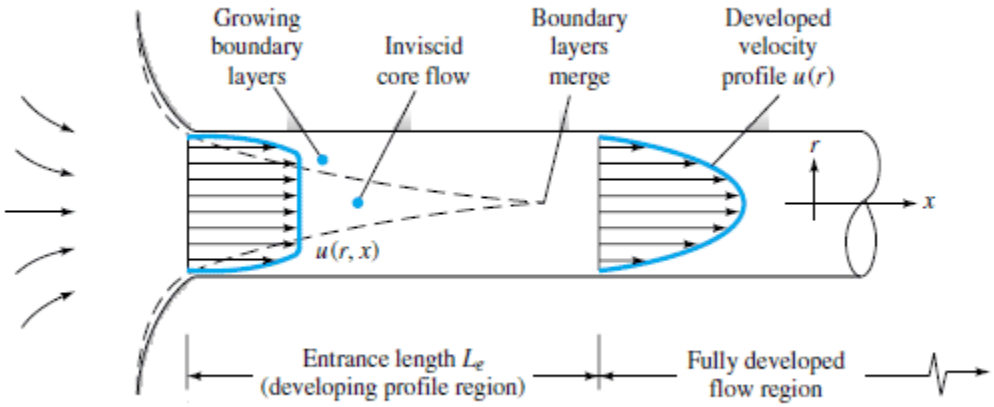

***Figure 11**: Velocity flow profile for Newtonian fluid [58].*

A non-dimensional parameter used to characterize the behavior of flow is Reynolds number defined as the ratio of inertial forces to viscous forces.

$$\mathrm{Re} = \frac{\text{inertial forces}}{\text{viscous forces}} = \frac{\rho v L}{\mu} \tag{4}$$

where ρ is the density of the fluid, v is the velocity (m/s), L is the characteristic length or hydraulic diameter (m) and μ is the dynamic viscosity of the fluid (Pa-s). If the Reynolds number is less than the critical Reynolds number which is 2500 for pipes, then the flow is laminar.

When the fluid enters the pipe, it starts slowly developing the boundary layers due to the zero velocity at the walls of the pipe and after a certain length, the flow profile is a parabola as shown in ***Figure 11*** and it will retain this parabolic shape until the end of the pipe. The length at which the flow is still developing itself is called the characteristic length which is dependent on the Reynolds number.

3.1.1 Newtonian fluids

If the fluid is a Newtonian liquid, the shear stress will be the product of the viscosity and the shear rate of the fluid introduced by Sir Isaac Newton for the first time in 1687 [59]. Viscosity is the measure of resistance of the flow and shear rate is the ratio of the velocity to the radius of the pipe. The product of viscosity and shear rate gives the shear stress [60]

$$\tau_{yx} = \mu\left(-\frac{dV_x}{dy}\right) = \mu\dot{\gamma}_{yx} \tag{5}$$

Viscosity of Newtonian fluids is always calculable regardless of the type of forces acting on it except for thermal changes. Even in response to temperature and pressure variations, viscosity changes in Newtonian fluids can easily be predicted. Examples of Newtonian fluids are water, honey, milk and some organic solvents like alcohol.

3.1.2 Non-Newtonian fluids

For the Newtonian flow, viscosity has a linear relationship with the shear rate. On the other hand, most fluids, especially suspensions, show non-linear behavior of viscosity which is dependent on the shear rate or shear rate history at constant temperature except the Ideal Bingham fluids which are strictly non-Newtonian fluids but once enough stress is applied, they behave as Newtonian fluids with a linear relationship between shear stress and shear rate. Velocity and shear stress profiles for a Bingham flow inside a pipe are given in ***Figure 13***. Non-Newtonian fluids can generally be divided into two types, plastic and dilatant fluids, depending on their relationship with shear stress as given in ***Figure 12***. Dilatant fluids are shear thickening fluids which means that the viscosity of the fluid increases with the shear rate, for instance, corn starch.

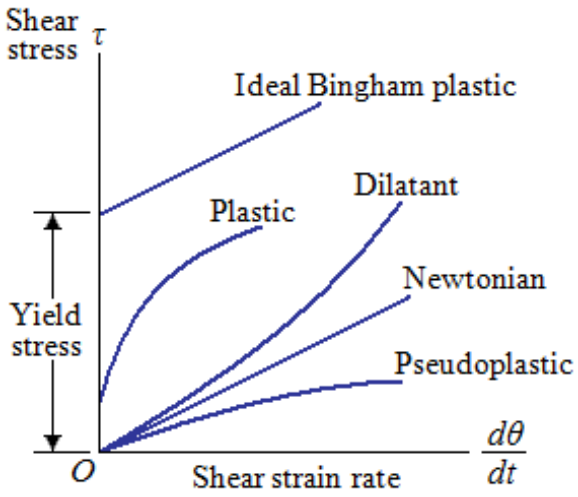

Figure 12: *Relation between shear stress and shear rate for Dilatant, Newtonian and Pseudoplastic flows.*

Pseudoplastic fluids, also known as shear thinning fluids are characterized by apparent viscosity as a decreasing function of shear rate and examples of such fluids are ketchup, mayonnaise etc. Non-Newtonian fluids are also known to change the flow profiles when flowing in the pipe. For Newtonian flows, velocity profiles are parabolic inside a pipe if the flow is laminar but velocity profiles are plug-shaped, i.e., velocity is constant in the center of a pipe and changing rapidly towards the end of capillaries for non-Newtonian fluids, see ***Figure 14***. Velocity profile for the shear thickening fluid is somewhat similar to the Newtonian fluid except it has pointed shape in the middle of the pipe. Since the velocity profile for the Pseudoplastic fluid is very similar to the Bingham flow, so it can be expected that the velocity gradient, i.e., shear rate, and shear stress for shear-thinning fluid should also be similar inside the pipe.

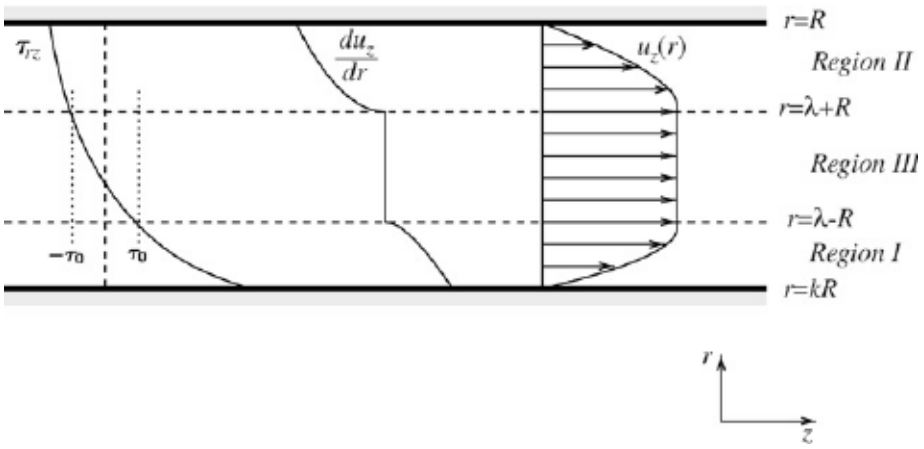

Figure 13: *Flow profile for a Bingham fluid in a capillary of radius R, where u and τ are the velocity and shear stress in fluid layers at a radial distance r from the center. τ_0 is the yield stress where the plug flow region ends. i.e., at radius of the plug flow region where r = λ+R or λ-R. [61].*

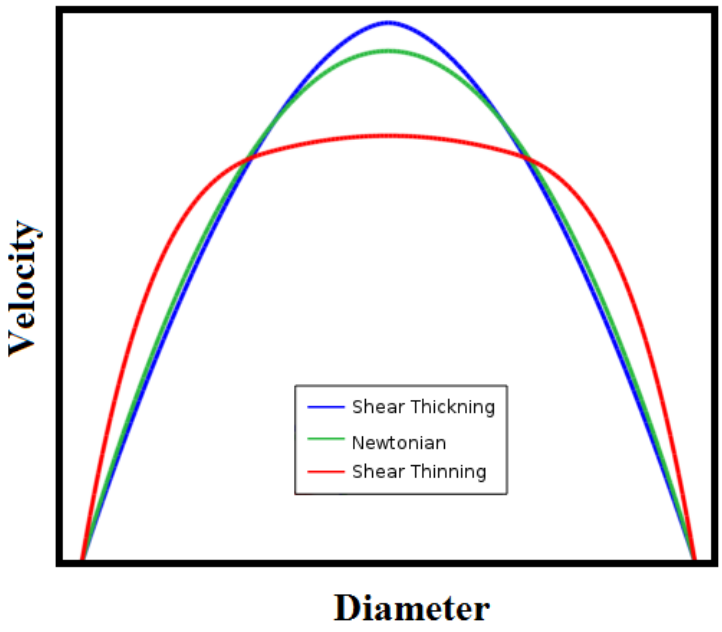

Figure 14: *Velocity profile comparison for Newtonian and non-Newtonian fluids (produced in COMSOL software).*

3.2 CONSTITUTIVE EQUATIONS FOR NEWTONIAN FLUIDS

A continuum body with the reference configuration B is said to be an ideal fluid if it satisfies the three conditions: (1) the mass density $\rho(\boldsymbol{X})$ is constant, i.e., $\rho_0(\boldsymbol{X}) = \rho_0 > 0$, (2) the material is incompressible meaning $\nabla^x \cdot \boldsymbol{v}(\boldsymbol{x}, t) = 0$, where $\boldsymbol{v}$ denotes the velocity and (3) the Cauchy stress field $\boldsymbol{S}$ is Eulerian which means that there is a scalar field $p(\boldsymbol{x},t)$ called the pressure such that $\boldsymbol{S}(\boldsymbol{x},t) = -p(\boldsymbol{x},t)\boldsymbol{I}$. A constitutive model for a Newtonian fluid is quite similar to the ideal fluid except that the Cauchy stress tensor $\boldsymbol{S}$ is Newtonian which means that there is a scalar field pressure $p(\boldsymbol{x},t)$ and a constant tensor $\boldsymbol{C}$ such that

$$\boldsymbol{S} = -p\boldsymbol{I} + \boldsymbol{C}(\boldsymbol{\nabla}^{\boldsymbol{x}}\boldsymbol{v}) \tag{6}$$

the tensor $\boldsymbol{S}$ depends on the viscosity of the fluid in the form of $\boldsymbol{C}(\boldsymbol{\nabla}^{\boldsymbol{x}}\boldsymbol{v}) = 2\mu sym(\boldsymbol{\nabla}^{\boldsymbol{x}}\boldsymbol{v})$, where μ is a constant called the absolute viscosity of the fluid and if this term is zero, the model will be reduced to ideal fluids. Setting the property of Newtonian fluids in balance of linear equation, one can obtain a set of Navier-Stokes equation for a Newtonian fluid given as

$$\begin{gathered} \rho_0 \left[\frac{\partial \boldsymbol{v}}{\partial t} + (\boldsymbol{\nabla}^{\boldsymbol{x}}\boldsymbol{v})\boldsymbol{v}\right] = \mu\Delta^{\boldsymbol{x}}\boldsymbol{v} - \boldsymbol{\nabla}^{\boldsymbol{x}}p + p_0\boldsymbol{b} \\ \boldsymbol{\nabla}^{\boldsymbol{x}} \cdot \boldsymbol{v} = 0 \end{gathered} \tag{7}$$

The Navier-Stokes equations govern the motion of fluids and can be seen as Newton's second law for fluids. When the spatial acceleration term is neglected, the above equations take the form of Stokes equations. They provide an approximate system of balance of equations appropriate for motions which are nearly steady and slow and which have small velocity gradients [62].

$$\begin{gathered} \mu\Delta^{\boldsymbol{x}}\boldsymbol{v} - \boldsymbol{\nabla}^{\boldsymbol{x}}p + p_0\boldsymbol{b} = \boldsymbol{0} \\ \boldsymbol{\nabla}^{\boldsymbol{x}} \cdot \boldsymbol{v} = 0 \end{gathered} \tag{8}$$

The main difference between an ideal fluid and Newtonian fluid is that the latter develops shear stresses [62].

3.2.1 Initial boundary value problem

An initial boundary value problem for a Newtonian fluid is a set of equations describing the motion of the body subjected to specified initial conditions in $\boldsymbol{D}$ at time $t=0$ and boundary conditions on $\partial\boldsymbol{D}$ for $t > 0$ is given as

$$\begin{aligned} \rho_0\left[\frac{\partial}{\partial t}\boldsymbol{v} + (\boldsymbol{\nabla}^{\boldsymbol{x}}\boldsymbol{v})\boldsymbol{v}\right] &= \mu\Delta^{\boldsymbol{x}}\boldsymbol{v} - \boldsymbol{\nabla}^{\boldsymbol{x}}p + p_0\boldsymbol{b} \quad \text{in} \quad \boldsymbol{D}\times[0,T], \\ \boldsymbol{\nabla}^{\boldsymbol{x}}\cdot\boldsymbol{v} &= 0 \quad \text{in} \quad \boldsymbol{D}\times[0,T], \\ \boldsymbol{v} &= \boldsymbol{0} \quad \text{in} \quad \partial\boldsymbol{D}\times[0,T], \\ \boldsymbol{v}(\cdot,0) &= \boldsymbol{v_0}(\cdot) \quad \text{in} \quad \boldsymbol{D}. \end{aligned} \tag{9}$$

The first equation is the balance of linear momentum equation and the second equation is the incompressibility constraint. The standard boundary condition for a Newtonian fluid is different than the one for ideal and elastic fluids. In this case all components of velocity, normal as well as tangential, must vanish at a fixed boundary. Just as for ideal and elastic fluids, the normal component vanishes because fluid cannot penetrate the boundary. In contrast to that, the tangential components must vanish at the boundary. The third equation $(9)_3$ is the so-called no-slip boundary condition that expresses the fact that the fluid cannot slip or cross along the boundary of D. This condition describes the interface between the Newtonian fluid and a fixed solid. If the solid boundary is movable, then there must be a prescribed value for the velocity [62].

3.3 VISCOSITY MODELS FOR NON-NEWTONIAN FLOWS

3.3.1 Power law

Power law relation between shear rate and shear stress is given as

$$\tau_0 = K\dot{\gamma}^n \tag{10}$$

Where *K* is the flow behavior index and *n* is a consistency index which is less than 1 for Pseudoplastic and greater than 1 for Dilatant fluids. From Equation (5), one can see that the relationship between viscosity and shear rate is the same as the power law for Newtonian fluids when *n* is one. *K* increases if the fluid is more viscous and decrease in the consistency index below one shows more thinning behavior of a fluid. This is the most commonly used model for the estimation of viscosity because it is quite easy to make the calculations for flow fields using Newtonian fluid constitutive equation. However, this model does not give any information about the infinite and zero shear rate viscosity of shear thinning fluids.

3.3.2 Carreau model

Another model which is used for the estimation of apparent viscosity is the generalized Newtonian Carreau-Yassuda viscosity function given as

$$\frac{\mu - \mu_{inf}}{\mu_0 - \mu_{inf}} = (1 + (\lambda\dot{\gamma})^2)^{\frac{n-1}{a}} \tag{11}$$

Where μ_{inf} is infinity shear rate viscosity, μ_0 infinite rate viscosity, λ relaxation time, *n* the power law index and a is the shape parameter. Carreau fluid is a generalized fluid model that behaves as a Newtonian flow at low shear rates and depicts the non-Newtonian behavior at high shear rates. It has been reported that some studies using the Carreau model have ignored the infinity shear rate viscosity as usually they are low in magnitude and difficult to obtain experimentally [63].

3.4 FINITE ELEMENT METHOD

All space- and time-dependent physical phenomena existing in nature can be written in the form of partial differential equations. It is very difficult if not possible to find exact solutions of these equations due to the complex geometries and problems. Hence, approximate solutions for such problems is obtained by solving the governing partial differential equations by using numerical

methods. The fundamental idea of the finite element method is to discretize the domain into several subdomains known as finite elements and partial differential equations are then written for each of these elements in a weak formulation [64].

The concept of discretization can be illustrated by using a simple example. Let's take a function u that is a dependent variable on certain length x in a partial differential equation. This function can be approximated by using another function u_h which is a combination of linear functions given as

$$u_h(x) = \sum_i u_i \psi_i(x) \tag{12}$$

where u_i are the coefficients of the functions corresponding to u and ψ_i are the linear basis functions for the approximation. The subscript i denotes a node on the length which is divided into a certain number of equal spaces.

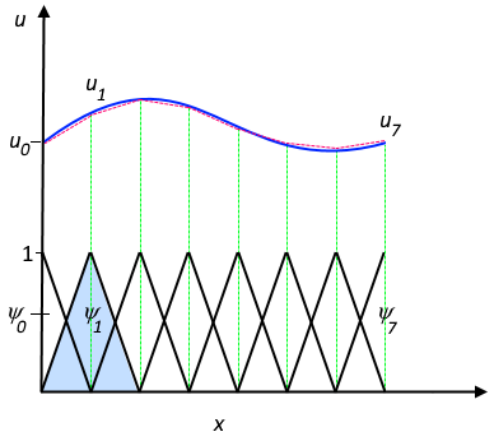

Figure 15: *The function u (blue solid line) approximated by u_h (red dashed line). Black lines at bottom are representing the basis function for each element [64].*

The linear basis functions have value 1 at their respective nodes and 0 at all other nodes. ***Figure 15*** shows that how the function u_h has approximated the function u by using only seven elements of the given length. The basis functions can be of higher order and the length domain can also be divided into unequal spaces. Some types of three dimensional mesh elements are given in ***Figure 16***. For 2D, the mesh elements are triangular and rectangular.

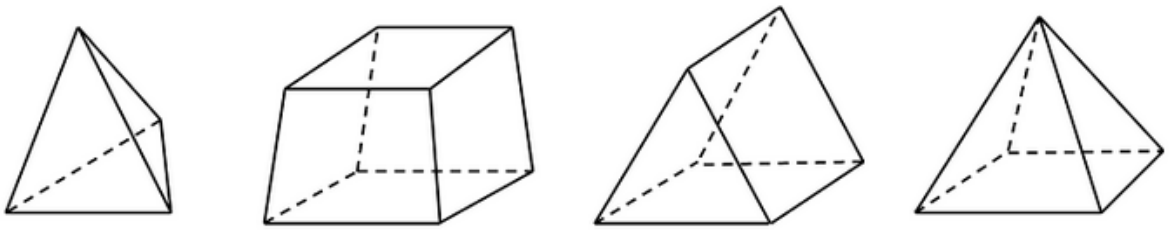

Figure 16: *3D mesh elements: tets, bricks, prisms and pyramids from left to right in order [66].*

Similarly, this procedure can also be applied to fluid flow modeling. Due to the complex nature of Navier-Stokes equations, only limited number of analytical solutions are available for parallel plates and pipes provided that the fluid flowing in these geometries is also simple such as Newtonian fluid. Velocity and pressure of fluids flowing in a complex geometry can only be predicted by using numerical methods. The module which particularly deals with the flow problems in fluid mechanics by using numerical methods is known as computational fluid dynamics (CFD). A number of CFD-based software are available in the market such as COMSOL, OpenFoam and Ansys etc., that allow users to simulate flow problems of wide range complexities.

4 MODELING

In the wet spinning process, fibrils align themselves in the direction of the flow when the suspension is passing from the capillary tube. It is important to visualize the effects of the parameters affecting the flow profiles of the CNF suspension in the capillary tube as well as how they are influencing the alignment of fibrils. In these simulations, the CNF suspension (fibrils and fluid) flowing inside the capillary tube is considered as one homogeneous fluid. It is assumed that fibrils do not affect the flow and density of the fluid used for the preparation of the suspension. Therefore, the density of the fluid used in the simulations is taken same as for water because water is used to prepare the CNF suspensions. Since the fluid is assumed to be homogenous with CNF fibrils uniformly distributed in the hydrogel, the flow in the capillary tube can be further assumed to be incompressible implying that the density remains constant in an infinitesimal volume.

4.1 PREPARATION OF CNF SUSPENSIONS

Four suspensions were prepared in the study conducted by Mohammadi ranging from 1.36 to 4 % w/v [16]. Hydrogel was prepared from never-dried birch pulp consisting of 24% hemicellulose content using a fluidizer (Microfluidics Corp., Newton, MA, U.S.A.). For the suspensions above 2.5 % w/v, mild stepwise centrifugation and homogenization was used to make the hydrogel more homogeneous and non-flocculated.

The rheological data for suspensions with concentration 1% and 2% w/v is also taken from another study and included in the simulation [21]. These suspensions were also prepared in the same manner as described above using never-dried, bleached, refined birch fibers fluidized with microfluidizer and diluted with deionized water.

4.2 PARAMETRIC STUDY

Four parameters are considered to observe their effects on flow profiles. These parameters include flow rate, concentration of CNF in the suspension, length and diameter of the capillary tubes. The same parameters were also used in an experimental study conducted in Aalto University [16]. The values of those parameters were also kept the same as used in the experimental study to make it

easier to provide a basis for validation of the simulation results. Two linear flow rates of 15 cm/min to 150 cm/min inside the capillary tube were used for the spinning of fibers. In simulations, one more linear flow rate in the middle of given flow rates (82.5 cm/min) is included in order to observe clear effects of flow rate on profiles. Flow rates are designated by FR1, FR2 and FR3 in the results section corresponding to 15, 82.5 and 150 cm/min flow rates. Capillary tubes of internal diameters of 0.4 mm, 0.5 mm, 0.75 mm and 1 mm and lengths of 20 mm, 200 mm and 1500 mm are considered in the simulations. These internal diameters are represented as ID400, ID500, ID750 and ID1000. Finally, four hydrogels of 1.36, 2, 3, 4 % w/v designated as CNF1.36, CNF2, CNF3 and CNF4 were used in the current study. Two more hydrogels of 1 and 2 % w/v prepared by Lunda are also included in this study. These parameters are changed systematically to see their effects on the flow behavior inside the capillary tubes.

4.3 COMSOL MODEL

COMSOL Multiphysics Version 5.2 ®, a FEM-based software, has been used to create all the geometries and to carry out the simulations.

4.3.1 Geometry

In the experimental study [16], the fibers were spun by using a setup where CNF hydrogels were delivered by using a pump from a funnel of 10 mm length with diameter varying from 5 mm to 1 mm into a capillary tube (shown in ***Figure 17***) of given diameter which leads to a coagulation bath filled with ethanol. Complete experimental setup is presented in ***Figure 4*** in Chapter 2.

Inlet was chosen at the beginning of funnel and outlet was selected at the end of the capillary tube. Since all the geometries are cylindrical in shape and the results remain the same in the circumferential direction, the geometrical domain is simplified to 2D axisymmetric geometry shown in ***Figure 18***, which has also improved the efficiency of the simulations by saving s lot of computational time. It is also important to add here that the results in the circumferential direction remains constant only for laminar flows and symmetry geometry condition (r = 0) is not valid for turbulent flows.

Figure 17: *Model Domain.*

4.3.2 Definition

COMSOL uses the Navier-Stokes equation and continuity equation to quantify the behavior of the flow. In these equations, $\boldsymbol{u}$ denotes the velocity, ρ is the density of the fluid, μ is the viscosity of the fluid and p is the pressure of the flow.

$$\rho\frac{\partial \boldsymbol{u}}{\partial t} - \nabla \cdot \mu(\nabla \boldsymbol{u} + \boldsymbol{\nabla u}^T) + \rho \boldsymbol{u} \cdot \nabla \boldsymbol{u} + \nabla p = 0$$
$$\nabla \cdot \boldsymbol{u} = 0 \tag{13}$$

And the viscosity of the non-Newtonian fluid will be predicted by an in-built viscosity model, i.e., the Carreau model given as

$$\mu = \mu_{inf} + (\mu_0 - \mu_{inf})(1 + (\lambda\dot{\gamma})^2)^{\frac{n-1}{2}} \tag{14}$$

where μ_{inf}, μ_0, λ, n are constants to be determined from the experimental data. The shear rate for the model is also pre-defined in COMSOL for axis-symmetric coordinates.

$$\dot{\gamma} = \sqrt{\frac{1}{2}\left((2u_r)^2 + 2(u_z + v_r)^2 + (2v_r)^2 + 4\left(\frac{u}{r}\right)\right)}$$

Most of the required output parameters like velocity, viscosity, shear rate, Reynold's number etc, are readily available in COMSOL but shear stress for the fluid was not defined among those parameters. The suspension is a non-Newtonian fluid but Carreau-fluid is a generalized Newtonian model. Therefore, shear stress can be defined as a product of shear rate and viscosity which, in turn, is dependent on the shear rate. Using expressions (5) and (14), the shear stress can be defined as

$$\tau = \dot{\gamma}\left(\mu_{inf} + (\mu_0 - \mu_{inf})(1 + (\lambda\dot{\gamma})^2)^{\frac{n-1}{2}}\right) \tag{15}$$

4.3.3 Boundary conditions

The given boundary conditions for assuming the axisymmetric geometry consisting of the funnel and capillary tube is presented in ***Figure 18***.

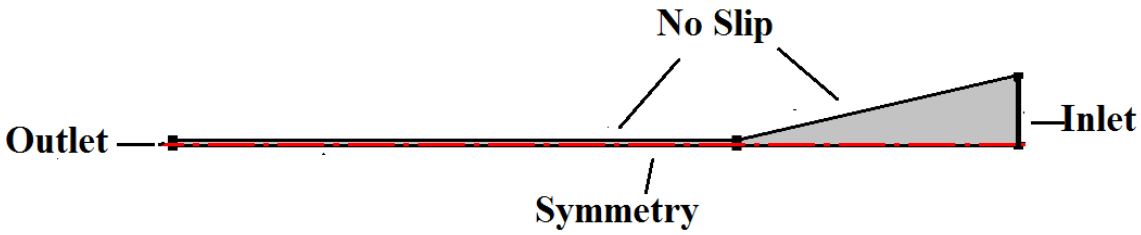

Figure 18: *Axisymmetric domain.*

Laminar inflow was described at the inlet and zero pressure condition was set at the outlet. The walls of the capillary tube had no slip condition, which implies that the velocity near the wall will be zero. The symmetry condition was given at the center of the capillary tube, i.e., at r = 0.

4.3.4 Mesh type

The default mesh given in COMSOL consists of triangular elements ranging from extremely fine to extra course. Default mesh did not give the required resolution inside the capillary tube and triangular mesh required high computation time. This is why they were replaced by mapped (structured) quadrilateral elements and the number of elements along the radius of the capillary tube were changed manually to produce the high-quality results as depicted in ***Figure 19***.

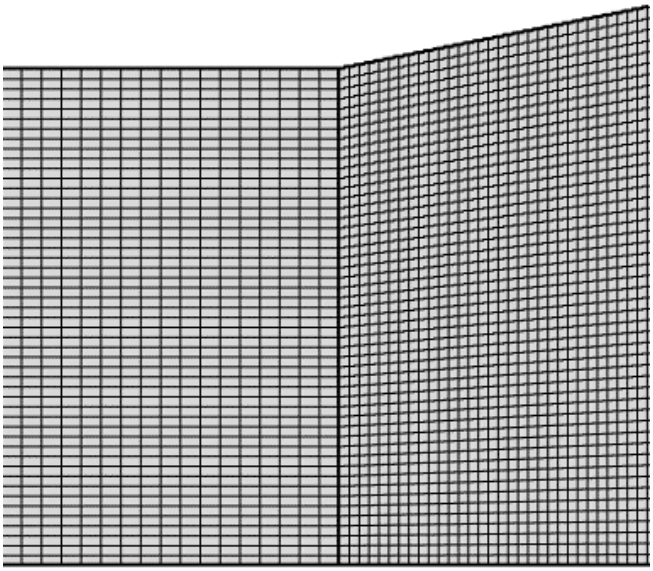

Figure 19: *Mapped quadrilateral elements created with COMSOL mesh tool (zoomed-in at junction with the tube and funnel on the left and right side, respectively).*

This picture is taken from the point where the capillary tube and the funnel meet and zoomed in since the geometry is really small. Since the reliability of the numerical model depends on the convergence of the solution, mesh analysis was run to check that if the solution is independent of the mesh size. The solution was converged after using only 8 elements per radius and the mesh elements along the radius were increased up to 100 elements per radius to improve the resolution of the output graphs.

4.4 CARREAU MODEL FITTED PARAMETERS

The relationship between the shear rate and viscosity is highly non-linear because of highly thixotropic nature of the suspension. Two principle models are given for generalizing the non-Newtonian flow in COMSOL: Carreau model and power law model. Power law for shear thinning fluids depicts that increase in the shear rate will decrease the effective viscosity indefinitely resulting in a fluid with infinite viscosity at rest and zero viscosity as the shear rate approaches infinity. But real fluids do not behave in this manner rather they have upper and lower limits for the viscosity corresponding to infinite and zero shear rates.

TABLE 1. CARREAU MODEL PROPERTIES.

CNF concentration	**Infinite shear viscosity,μ_{inf} (Pa-s)**	**Zero shear viscosity, μ_0 (Pa-s)**	**Lambda, λ (1/s)**	**n**	**μ_0/λ**
CNF1.36	0.0107	9134	297	0.117	31
CNF2	0.022	23664	308	0.113	77
CNF3	0.1007	93156	415	0.093	225
CNF4	0.3822	201249	498	0.0757	404

Carreau model well describes the shear thinning behavior by generating constant values for low and high shear rates as shown in ***Figure 20***. Carreau model has also been used successfully in the past for modelling the non-Newtonian suspension behavior [46] to quantify the behavior of CNF hydrogels and therefore it has been chosen here for quantifying the viscosity of the fluid. Four suspensions have been used here with concentrations 1.23%, 2%, 3% and 4% and their rheological

data has been obtained from the experiments performed by Mohammadi [16]. The Carreau model parameters are obtained by plot-fitting the graphs in Microsoft Excel and they are listed in **Table 1**.

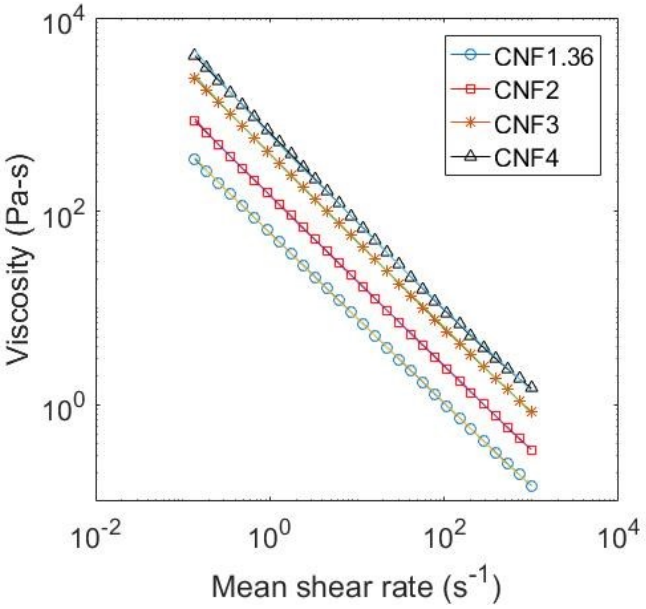

***Figure 20**: Apparent viscosity with solid lines representing rheological data of CNF suspensions with concentration 1.23, 2, 3 and 4 % w/v and marker lines are the corresponding Carreau fit to the data.*

5 RESULTS AND DISCUSSION

5.1 BEHAVIOR OF NON-NEWTONIAN FLOW

COMSOL results are meeting the expected results for the velocity in the capillary tube, i.e., the profile is flat in the middle and decays rapidly towards the walls as shown in ***Figure 21*** and the relationship between the shear stress and shear rate is similar to the behavior of shear thinning fluids discussed earlier in Chapter 3.

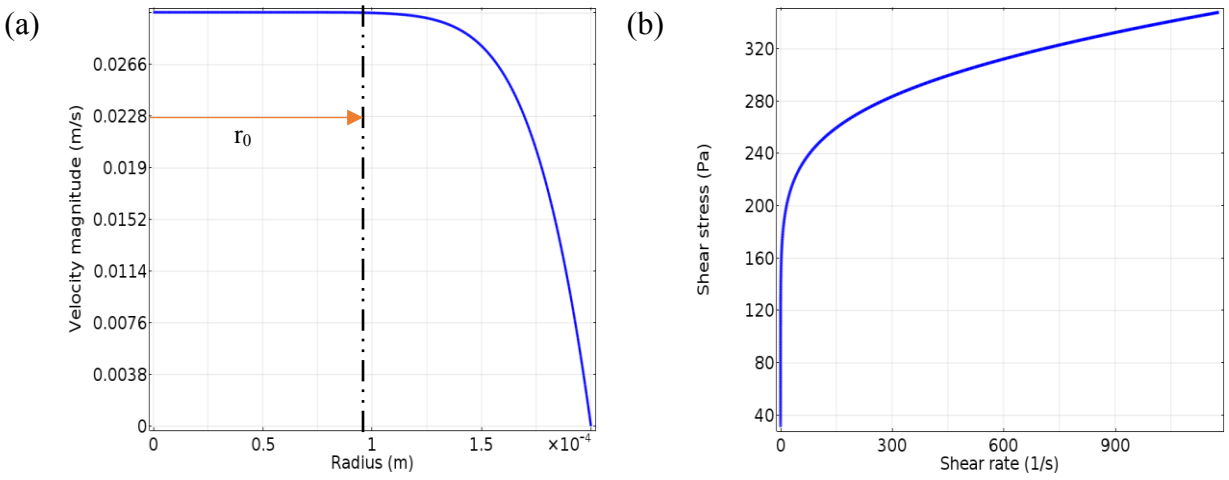

Figure 21: *Domain and Flow Profiles: Velocity field (red and blue color corresponds to highest and lowest velocity, respectively.* ***(a)*** *Magnitude of the velocity field in the capillary tube from the simulations, r_0 is the radius for which velocity is nearly constant, and r is the radius of the capillary tube* ***(b)*** *Characteristic graph for the shear thinning fluids, i.e., Shear stress profile plotted against shear rate.*

5.1.1 Problems with boundary conditions

Before discussing the results further, it is important to point out the problems encountered during simulating the flow of hydrogels in COMSOL. In the beginning, the boundary condition described at the inlet was laminar flow rate and it gave smooth velocity profiles but the shear stress profiles had a marked deviation near the center of the capillary tube even though the overall trend was meeting the expectations (see the expected shear stress profile for a shear thinning fluid demonstrated in ***Figure 13***, Chapter 3) as it is evident from the ***Figure 22***. After running many simulations by varying parameters, both in flow properties and Carreau model parameters, it was first thought to be a problem because of the highly non-linear behavior of the given hydrogels and solution for viscosity profiles is not converged because of the mesh size as changing the mesh size resulted in reduction and amplification of the size of deviations in an irregular manner.

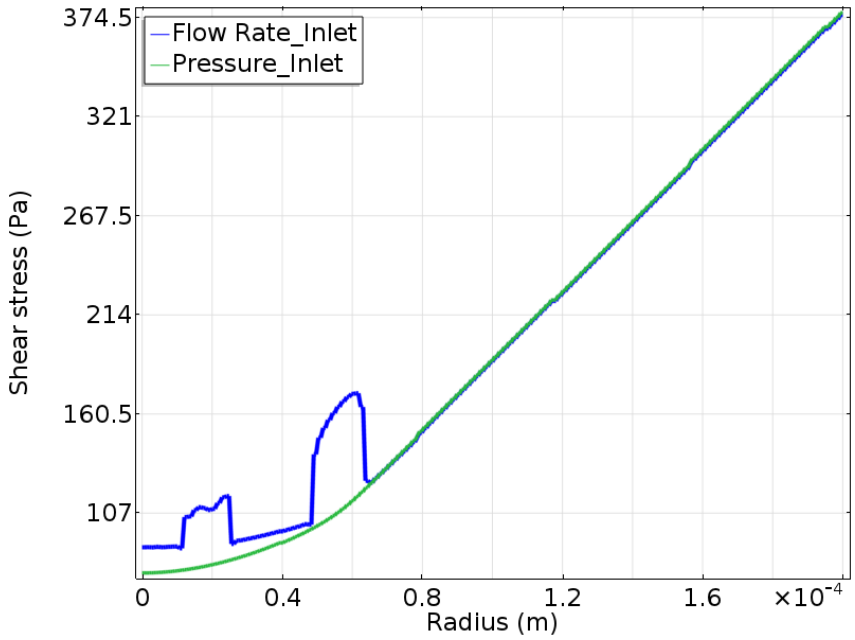

Figure 22: *Boundary condition effect on shear stress profiles: green plot is for pressure inlet and blue is for flow rate inlet.*

Other parameters like inlet and outlet boundary conditions were also varied to see their effect on the model and surprisingly, it was revealed that by changing the boundary condition at inlet from laminar inflow to pressure inlet, it resulted into a trend for shear stress which has been expected from the beginning (referring to ***Figure 13***). For this reason, the boundary condition was changed from laminar inflow to pressure on inlet in all the cases for different parameters and their values are listed in **Table 2** (see Appendix 2). Since there was no information available about pressures at the inlet, therefore pressures at inlet were obtained for all the cases by first simulating the problem with flow boundary condition and the corresponding values of pressure on the inlet were obtained. Then the simulation was run again by substituting the pressure inlet condition. Velocity and shear stress profiles are compared for both cases of inlet boundary conditions to ensure that the pressure obtained through this way is correct.

5.2 SENSITIVITY ANALYSIS OF CARREAU MODEL

All the parameters in the Carreau model were varied at an early stage of simulations to investigate their effect on the velocity profiles. For these suspensions, infinity shear rate viscosity μ_{inf} was so small that it was negligible in comparison to zero shear rate viscosity μ_0 which led to a speculation that there might be only two parameters in the Carreau model which are mainly affecting the behavior of the flow i.e. model parameter λ and zero shear rate viscosity μ_0. In the Carreau model, the infinity shear rate viscosity is neglected and the Equation (14) is reduced to the form

$$\mu = \mu_0(1 + (\lambda\dot{\gamma})^2)^{\frac{n-1}{2}} \tag{16}$$

For higher shear rates, $(\lambda\dot{\gamma})^2 \gg 1$ and for non-Newtonian fluids showing extremely shear thinning behavior $n \ll 1$ it can be said that the viscosity for the given suspensions is primarily proportional to two parameters, directly proportional to the zero shear rate viscosity and inversely proportional to the model parameter λ. The ratio of μ_0/λ has increased exponentially with the increase in concentration of fibrils. This ratio was varied between 6 to 400 Pa (smaller ratio corresponds to less concentration and higher ratio is for higher concentration) and it is quite clear in ***Figure 23-a***

that increase in this ratio has shifted the trend of velocity profiles from parabolic to plug flow implying that, with the increase in concentration.

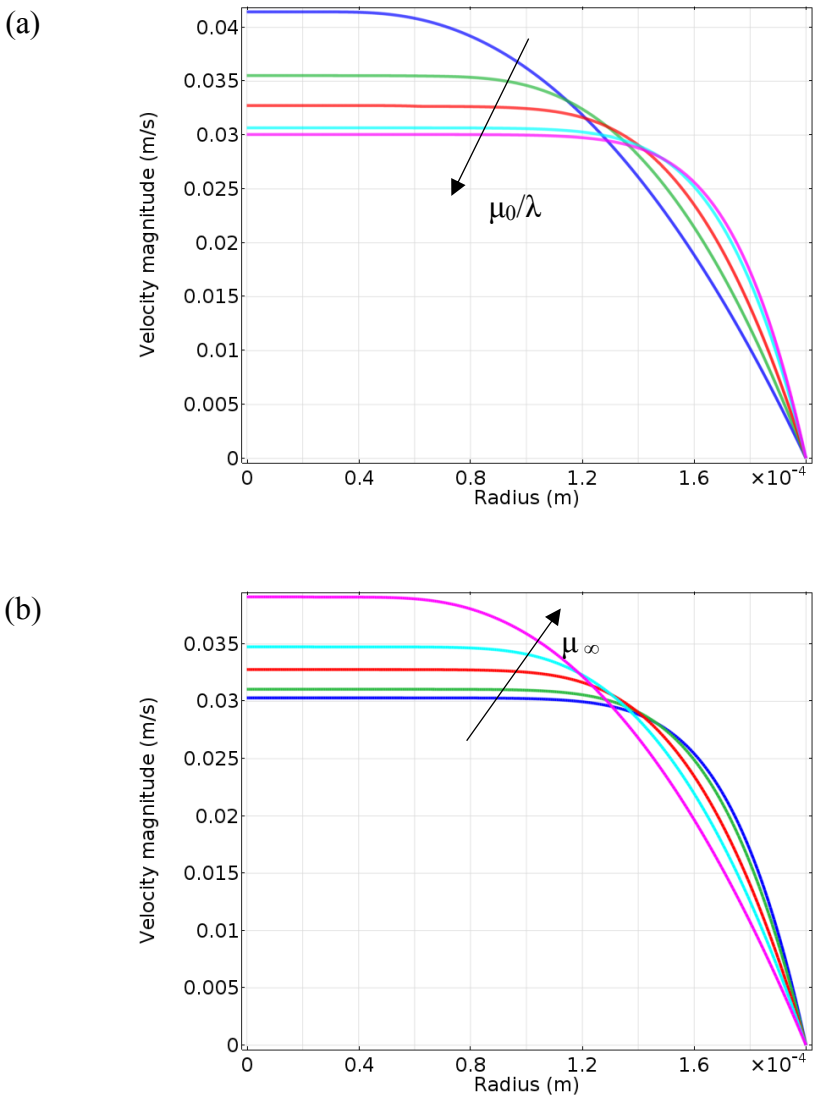

Figure 23: *Effect of Carreau model parameters on the velocity profiles:* ***(a)*** *Variation of ratio of zero shear viscosity to model parameter* ***λ (b)*** *Only increasing infinity shear rate viscosity using the same values for all other parameters in the Carreau model.*

(a)

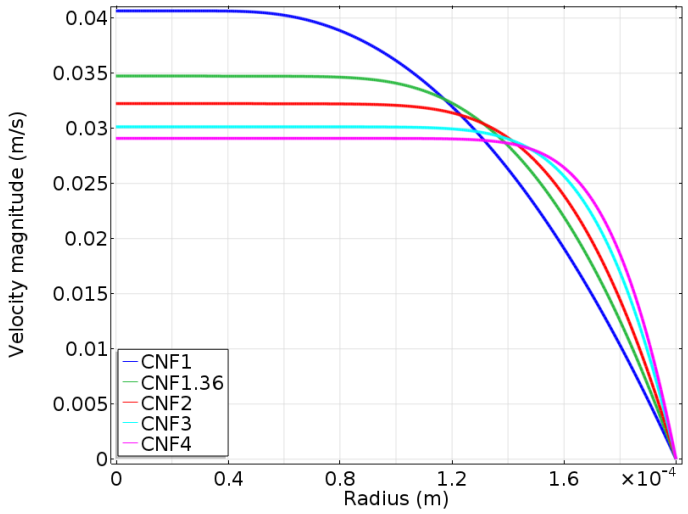

(b)

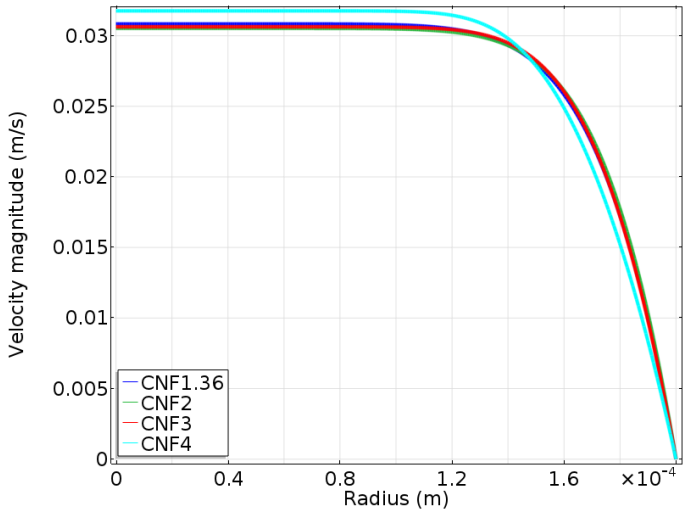

Figure 24: *Velocity Profiles:* ***(a)*** *velocity predicted by Carreau model keeping infinite viscosity constant* ***(b)*** *profiles with all the plot fit parameters of Carreau model.*

In the second step, model parameter *n* was also varied along with zero shear rate viscosity and λ and the resulting profiles are presented in ***Figure 24-a***. It is very interesting to see that the trend for velocity profiles remained exactly similar to the previous case where model parameter *n* was

neglected. Thirdly, infinity shear rate was also varied from 0.01 to 0.3 Pa-s by keeping all other parameters μ_0, λ and n constant to observe its effect on the model. It was surprising to find out that there was a huge difference in the flow profiles even with this small variation. ***Figure 23-b*** shows that increasing infinite shear rate has changed the velocity profiles trend from plug shape profiles to parabolic profiles.

All these parameter variations reveal that the Carreau model is very sensitive to very minute variations in any of the aforementioned parameters. Since all these parameters have been obtained by plot fitting of the given rheological data, smaller changes in the values of the rheological data can lead to drastic shifts in the shape of the velocity profiles.

5.3 PARAMETERS EFFECT ON VELOCITY PROFILE AND SHEAR RATE

5.3.1 CNF concentration in suspension

In the first parametric case, the concentration of hydrogels was varied from 1 to 4% by keeping other parameters constant such as the highest linear flow rate of 150 cm/s, the smallest diameter 400 μm and 2 cm length of the capillary tube was used in the simulations. 1.36% concentration is considered as the minimum concentration for the spinning of continuous fiber but in these simulations, a CNF suspension of 1% from another study is also included for comparison. There was no significant difference between the velocity profiles for different concentrations in the range between 1.36 to 4% (***Figure 33-a*** see Appendix 1). It was expected that velocity profile for the suspension with lower concentrations would be more like a parabolic profile since the suspension is less viscous and with higher concentrations the behavior would be closer to a plug flow because of higher suspension viscosity.

For the four hydrogels (CNF1.36, CNF2, CNF3 & CNF4) [16], results obtained for the velocity profiles from simulations did not match theoretical expectations for the effect of concentration on the velocity profiles for the hydrogels but the hydrogels for concentration 1 and 2% prepared by Lundahl [21] shows the expected results but unfortunately, the rheological data was available only for two concentrations. One possible reason is that the Carreau model is very sensitive to minute

changes in the model parameters as discussed in the previous section and human error cannot be overlooked while obtaining the rheological data.

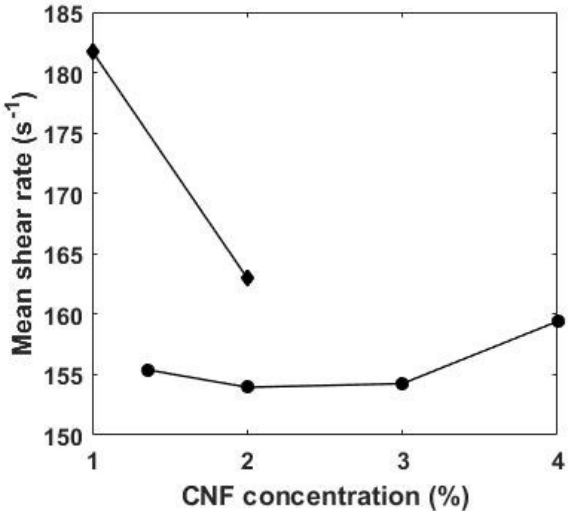

Figure 25: *Effect of CNF concentration on the shear rate, diamond markers are corresponding to the CNF hydrogels prepared in reference [16], [21] and circular coordinates are from reference [16].*

Since the main property of the flow which allows the fibrils to align in a shear flow is the shear rate. Therefore, the second factor analyzed situation was the velocity gradient or shear rate for different concentrations. Mean shear rate was obtained by integrating the area under shear rate profiles and was plotted against the shear rate as shown in ***Figure 25***. Diamond shaped markers in the figure are shear rates corresponding to the study [21] where the concentration of the fibrils was 1 and 2 % w/v which is quite high (shear rate has dropped from 182 to 163 s^{-1} with the increase in concentration). Two hydrogels (from [21] and [16]) with same concentration 2 % w/v have mean shear rates 163 and 154.5 s^{-1}. Explaining everything by mean shear rate is also challenging because the shear rate is constantly varying throughout the diameter of the capillary tube (***Figure 34-b***). It

is very clear that the regions closer to the walls of the capillary tube have shear rates much higher than the average shear rate. Shear rate for CNF2 has also gone higher than the CNF1 after 164 nm distance outward from the center of the capillary tube but nevertheless the shear rate for CNF1 is distributed as compared to CNF2, which further strengthens the fact that the velocity profile for the dope with concentration 1% w/v is more parabolic.

Mean shear rate remained almost constant for concentrations 1.36%, 2% and 3 % and then there is a small increase in the shear rate for CNF 4 from 154.5 s^{-1} to 164 s^{-1}. It might be the case that the suspensions below 2.5% were stable, homogeneous and non-aggregated. The Carreau model should only be used for homogeneous solutions as it does not take into account the complex behavior in the flow which arises because of the aggregation of suspensions. Although the mean shear rate for CNF4 is higher than for the others but if the shear rate graphs plotted for different concentrations (in ***Figure 33-b*** Appendix 1) are carefully looked upon, one can see that the velocity gradient for CNF4 is less steep than for the others closer to the walls of capillary tube.

Though the shear rate is almost the same for these three concentrations, increase in concentration up to certain extent, i.e., CNF2 and CNF3 (ultimate tensile strength of 300 MPa and Young's moduli of 17 GPa) in case of Mohammadi gave better mechanical properties when compared with the properties of CNF1.36 (ultimate tensile strength of 258 MPa and Young's moduli of 12 GPa) [16]. It was also reported that there spinning of fibers by using dope of 1% was challenging as it was not producing the continuous fibers [21]. This clearly shows that higher free volume of solids in the suspension also has an effect on the properties of spun fibers.

It can be concluded that the shear rate is not the only driving parameter for orientation in this case. Average viscosity and concentration of fibrils are also two important factors which contribute to the orientation of fibrils during the flow. Suspensions with higher concentrations showed higher viscosity (473, 1350, 3630, to 6970 Pa-s at lower shear rate of 0.1 s^{-1} corresponding to 1.36%, 2%, 3% and 4%) as well as suspensions with higher free volume of solids enhance mechanical properties of the spun fibers. Higher viscosity means more resistance to the flow and consequently more resistance to fibers from aligning but what should be the optimum limit of viscosity above which fibers will not align during the flow is not yet very clear. With increase in concentration, there is more interaction among the fibrils and to find an optimum value for the concentration when

fibrils are still free to move without affecting each other inside the flow which requires more experiments to be performed. This model also does not take into account the repulsive or attractive forces among fibrils in flow which may have a considerable influence on the flow behavior and orientation of fibers.

5.3.2 Diameter of capillary tube

Velocity and shear rate profiles for different diameters are shown in ***Figure 35*** in Appendix 1. There is a little difference of magnitude in the velocity of the smallest diameter, which can be because of the flow rate calculated at the inlet for laboratory experiments and may have a little error. The trend for velocity profiles for all diameters were plug-shaped and the constant velocity was distributed equally along the diameter of the capillary tube, i.e., ratio r_0/r (r_0 is the radius of constant velocity region from the center of capillary tube) remained constant for all the diameters.

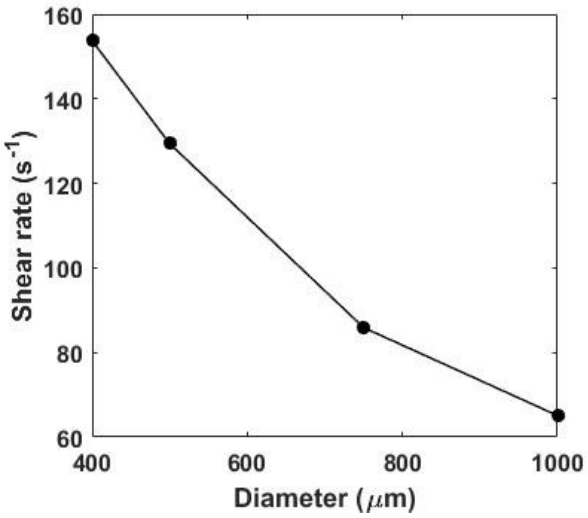

Figure 26: *Effect of the diameter on the shear rate.*

It is because the inlet flow variation for each diameter get the same linear flow rate inside the capillary tubes listed in **Table 2** (Appendix 2) but if the flow rate at the inlet is kept constant for all diameters, it will result in a more parabolic flow for shorter diameters. In short, it can be said

that it was not the parabolic shape of velocity profile which helped in better alignment of fibrils in shorter capillary tubes. Shear rate on the other hand is affected by the use of different diameter tubes. Decreasing the diameter from 1000 to 400 mm means that the shear rate has increased in the center of the capillary tube from 65 to 155 s^{-1}, as shown in ***Figure 26***. In the experimental study, the smallest diameter increased Young's modulus and yield strength 21 % and 36 %, respectively.

5.3.3 Flow rates for spinning

In ***Figure 36-a*** in Appendix 1, the effect of the flow rate magnitude is demonstrated. In the experimental parametric study [16], only two flow rates were used but in the simulations. the flow rate magnitude was varied between the given flow rate magnitudes. It is quite clear from the velocity profiles in ***Figure 36*** in Appendix 1 that the linear flow rate is increased linearly with the increase in inlet flow rate and the velocity profile also shifted its trend from plug to a bit more parabolic like with increase in velocity.

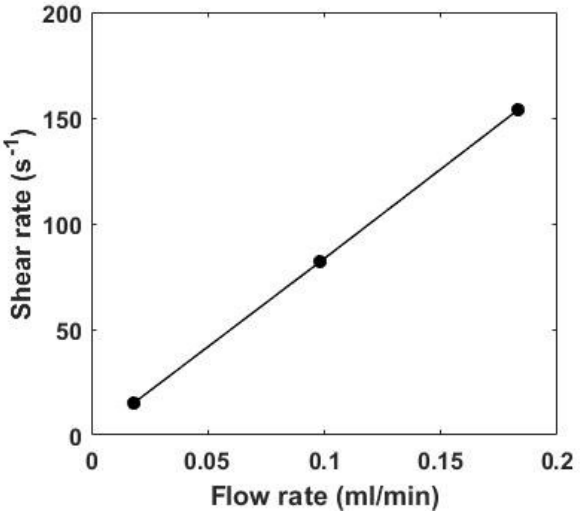

Figure 27: *Effect of the flow rate on the shear rate.*

The shear rate inside the capillary tube is increased linearly by increasing the flow rate, as demonstrated in ***Figure 27***. In this case, it is not just the mean shear which is higher for the higher flow rate but the shear rate is higher for the higher flow rate throughout the capillary section. In the

experimental results, a higher linear rate inside the capillary tube resulted in better orientation, higher tensile strength, yield strength and Young's modulus as compared to lower linear rate. Comparing this with the experimental results, it will be argued further in the subsequent sections that this is mainly because of the shear rate which helped in the alignment of fibrils.

5.3.4 Length of the capillary tube

In the experiments conducted in the laboratory, the length of the capillary tube seems to affect the alignment of fibers. The X-ray diffraction parameters revealed that the orientation parameter for the fibers spun from the longest and thinnest capillary with a high flow rate was as high as 0.762. Fibrils extruded from the longest capillary tube of the smallest diameter with a higher flow rate gave higher stiffness, tensile strength, Young's Modulus and yield point. Fibers extruded from a longer capillary tube were more circular and had both smoother surfaces and smaller diameters.

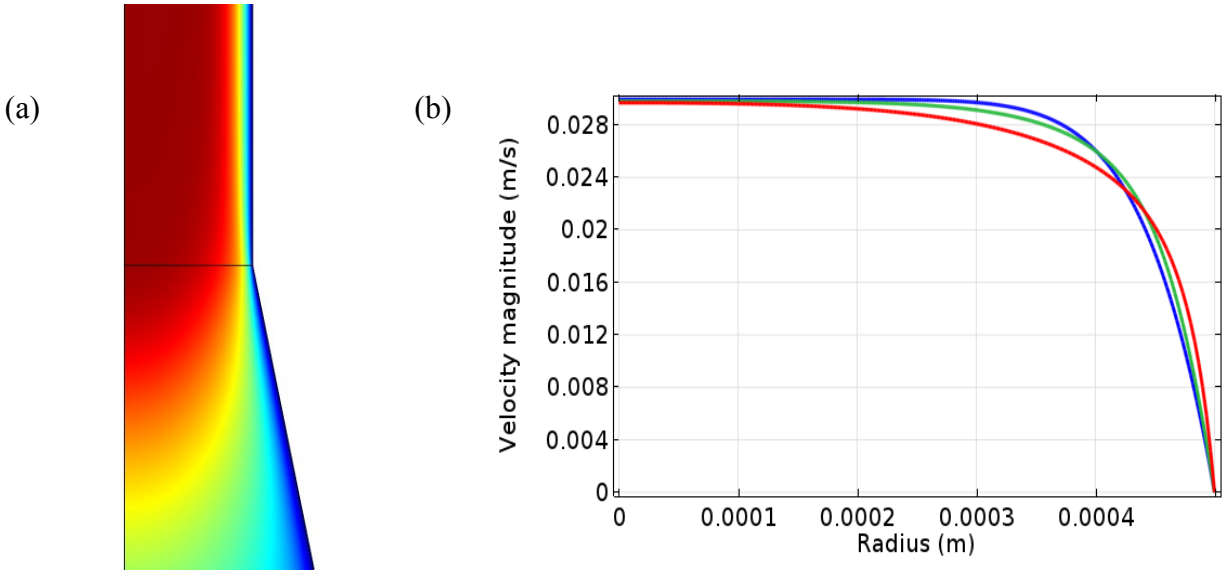

Figure 28: *Development of the flow in the capillary tube:* ***(a)*** *2D zoomed plot at the junction* ***(b)*** *1D plot with red line at the very beginning of capillary tube, green line at 0.25 mm from the starting line and blue line shows the fully-developed velocity profile.*

Theoretically speaking, the length of the capillary tube does not have any effect on the shape of velocity profiles or on the gradient of the velocity profiles. In the laminar flow, when the flow if fully developed, the flow profiles remain the same. In the simulation, it was observed that the velocity profile was immediately developed after the fluid enters into the capillary tube at 1 mm distance from the funnel, please see ***Figure 28***. The case presented in this figure is for the suspension CNF2 flowing with highest flow rate in 2 cm long capillary tube ID1000. According to the experiments, however, it seems that the fibrils need more residence time inside the capillary tube to achieve highest orientation. Since all the flow parameters remain constant for capillary tubes of different length, it is not possible to explain which flow parameter was actually responsible for the better alignment.

5.3.5 Relationship of shear rate and mechanical properties

In the previous section, we have observed that increase in the flow rate and decrease in the diameter has increased the shear rate inside the capillary tube. It has also been discussed that the mechanical properties were enhanced due to higher flow rates and smaller diameters. Fibers spun with the higher linear flow rate showed higher tensile strength, yield strength and Young's modulus (328 MPa, 139 MPa and 18.84 GPa, respectively), in comparison to the fibers extruded with the lower flow rate (296 MPa, 78 MPa and 12.6 GPa, respectively). It is important to mention here that the main parameter which aligns the fibrils is the shear rate. With increase in the flow rate, the shear rate is increased which results in better alignment of fibrils. Hence, in both cases, it can be concluded that the only parameter which affected the orientation of fibers was shear rate. To see the effect of the shear rate on the mechanical properties of fibers, yield strength (MPa), Young's modulus (GPa) and toughness modulus (MJ/m^3) obtained from the experimental study are plotted against the shear rate calculated in the previous sections as shown in ***Figure 29***. The mechanical properties plotted in this figure are corresponding to the experimental study for different diameters. Similarly, the shear rate is also taken from the simulations carried out for diameters by using the 2% CNF suspension and highest flow rate in the longest capillary tube. Yield strength and Young's modulus are both increased with the increase in the shear rate produced as a result of decreasing the diameter. The highest yield strength obtained was 150 MPa corresponding to the smallest diameter and the highest Young's modulus is 20 GPa.

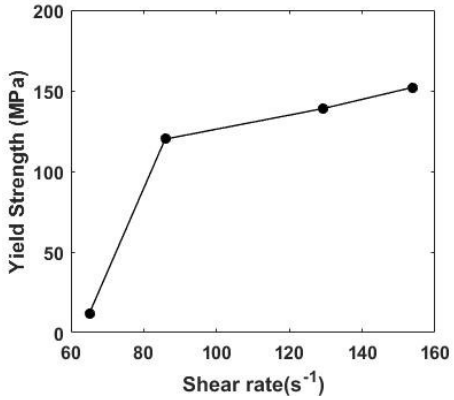

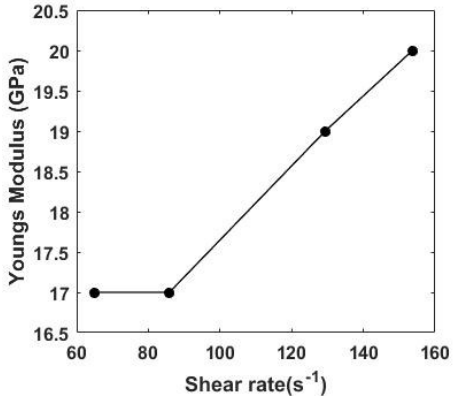

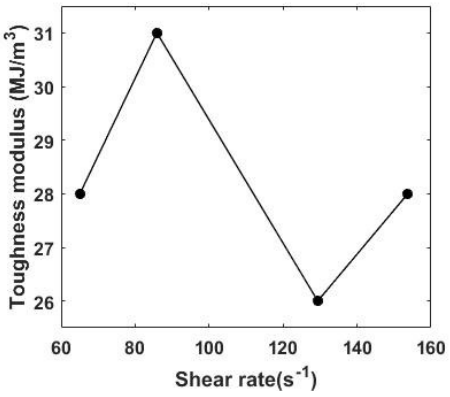

Figure 29: *Effect of the shear rate on the mechanical properties of spun fibers.*

Toughness modulus did not show any regular trend with the increase in the shear rate.

It should also be added here that different mechanical properties have shown different trends in response to increase in shear rate. Furthermore, a microscopy study revealed that there was not much qualitative difference seen between the core of fibers and the region around the surfaces and it was argued that the flow is not plug like rather it is distributed (velocity is varying throughout the section).

5.4 PARAMETERS EFFECT ON SHEAR STRESS

Although the shear stress has not any primary effect on the alignment of fibrils during the flow but still it is important to get an idea of the shear stress variation as a result of changes in different parameters. Shear stress inside the flow gives information about frictional forces existing between the layers of the fluid. Intuitively, alignment of fibers with high aspect ratio in a less viscous flow should be easier to achieve as compared to a flow with higher viscosity such as honey.

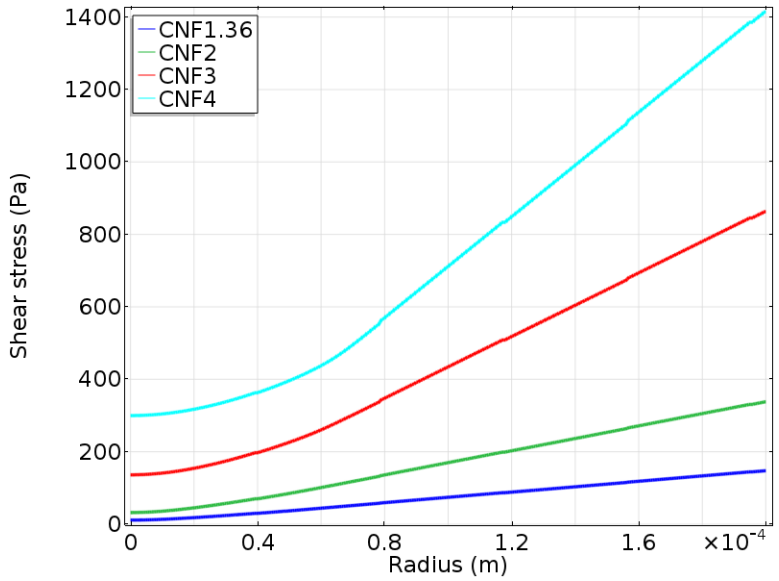

Figure 30: *Shear stress profiles for suspensions with nanofibrils concentration varying from 1.36% to 4% w/v in capillary tube ID200 with maximum flow rate.*

Stress profiles in the capillary tube shifted its trend from linear to non-linear when the concentration of the cellulose nanofibrils was increased in the suspensions as demonstrated in ***Figure 30***. Shear stress increases linearly along the radius in a pipe flow with zero shear stress at the center of the pipe and maximum on the walls for Newtonian flow but for non-Newtonian flow it is expected to have non-linear shear stress profiles as depicted earlier in ***Figure 13*** for Bingham flows. This could be presented as another guideline for the behavior of non-Newtonian suspension as shear stress profiles fluctuate between Newtonian and plastic fluid with the variation in the concentration of the fluid. Shear stresses have increased remarkably ranging from no stress to 300 Pa in the center of the capillary tube and 150 Pa to 1400 Pa when the concentration is increased from 1.36% to 4% w/v. It might be because of high frictional forces in the flow along with the increased fibril interactions that resulted in poor morphology of fibers spun using CNF hydrogel with 4% w/v concentration.

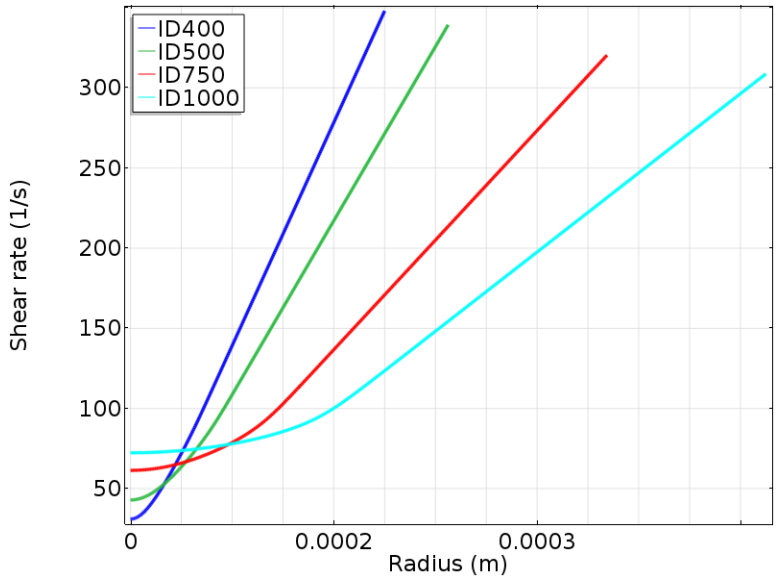

Figure 31: *Shear stress profiles in capillary tubes with different diameters ranging from 400-1000 nm keeping the flow rate (FR3) and concentration constant (CNF2).*

Shear stress is affected a little by the use of different diameter tubes, with increase in the diameter shear stress has increased in the center of the capillary tube (from nearly zero to 75 Pa) and decreased at the end of the diameter (350 Pa to 310 Pa) which means that the slope of the plot with smaller diameters is higher as compared to the slopes for the larger diameter shear stress plots. Shear stress profiles for different diameters are demonstrated in ***Figure 31***.

Similarly, change in the flow rate did not have a pronounced effect on shear stresses but it has shifted the trend of the profiles from linear to non-linear when increasing the flow rate, as shown in ***Figure 32***.

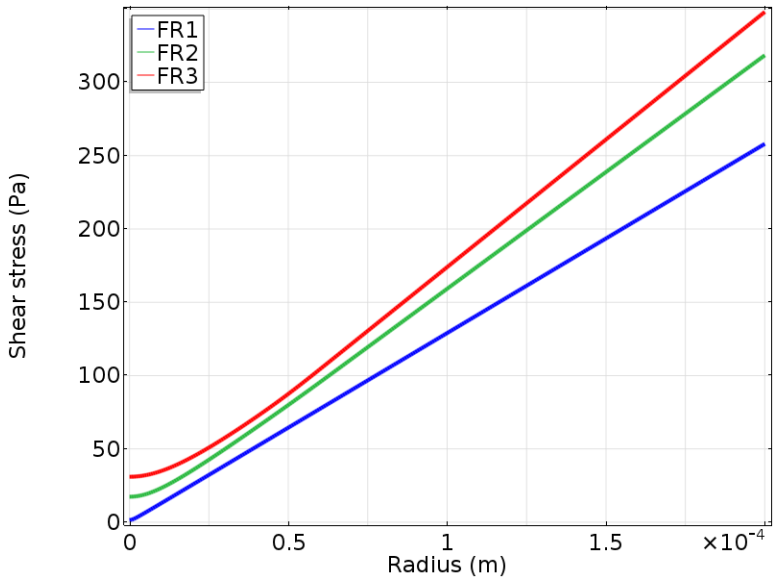

Figure 32: *Shear stress profiles for CNF2 in capillary tube ID200 for flow rate ranging from 15-150 cm/min.*

6 CONCLUSION

A systematic evaluation of the effect of different parameters on the flow conditions inside a capillary tube by using numerical simulation was conducted. Of particular interest is the linear flow rate, concentration of nanofibrils in suspensions, diameter and length of the capillary tube. The output flow parameters taken into account are velocity, shear rate and shear stress. The numerical model for the fluid flow uses a set of Navier-Stokes equations defining a boundary value problem and the model used for the prediction of non-Newtonian behavior of the cellulose nanofibrils suspension is the Carreau model. The flow under consideration was laminar and steady, and the fluid was assumed to be incompressible.

It was shown that the changes in these parameters, apart from the length of the capillary tube, had enormous effects on the shear rate and shear stress profiles of the flow but there was little effect observed on the velocity profiles. Changes in the diameter does not affect the shape of the velocity profiles but the mean shear rate was increased when decreasing the diameter. Similarly, the shear rate was observed to increase linearly with the increase in the flow rate throughout the diameter of the capillary tube. Changes in the length of the capillary tube did not have any effect on the flow profiles. In case of variation in the concentration of nanofibrils, it was expected that the suspensions with lower solid contents behave more like a Newtonian fluid flow and the velocity profiles for highly concentrated suspension should result in a plug like flow. Six suspensions were used to see the effect of the concentration and their rheological data was taken from two different studies: one set with two suspensions of 1% and 2%, and the second set with four concentrations ranging from 1.36 to 4%. In the former case, simulations of lowest concentration of 1% produced more like a parabolic profile, i.e., closer to Newtonian flow behavior, and with the higher concentration velocity profiles were more flattened in the middle but for the latter, changes in the concentration did not show a similar trend. Attempts were made to identify the reason behind such behavior by carrying out a sensitivity analysis for the Carreau model. It turned out that this model is very sensitive to minute changes in the values of parameters.

At the end, the results retrieved were compared with the mechanical properties and orientation of fibers obtained by using the same parameters documented in research papers. It was shown that the

main factor which was affected by the variation of the given parameters is the shear rate and consequently, it was because of the shear rate, the alignment of nanofibrils was increased in the experimental studies. Shear stress was increased by increasing the concentration and flow rate throughout the capillary tube, and decrease in the diameter changed the trend of shear stress profiles to non-linear. Altogether, higher shear rates result in higher Young's modulus and yield stress and higher shear rates can be obtained by decreasing the diameter and increasing the flow rate. The shear stress does not depend on the concentration.

Finally, it should be noted that there are many other factors reported in the literature which favor the alignment and mechanical properties of spun fibers besides the flow properties. For instance, interaction of fibrils during the flow, flocculation of the fibrils and increased free fibrils that cannot be prescribed by using the present approach focusing on fluid dynamics assuming homogeneous flow properties and relying on simplified versions of classical continuum theories. Other important issues that should be studied more carefully are the following: errors while collecting the rheological data and sensitivity of the parameters for the Carreau model.

APPENDIX 1 – VELOCITY AND SHEAR RATE PROFILES

Effect of Concentration

(a)

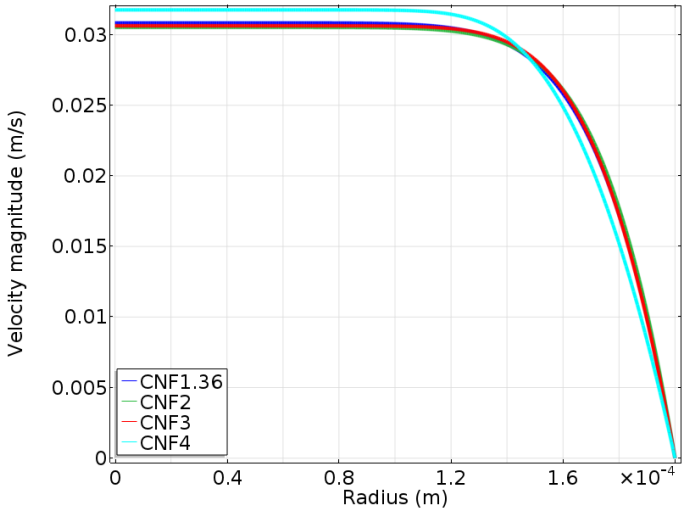

(b)

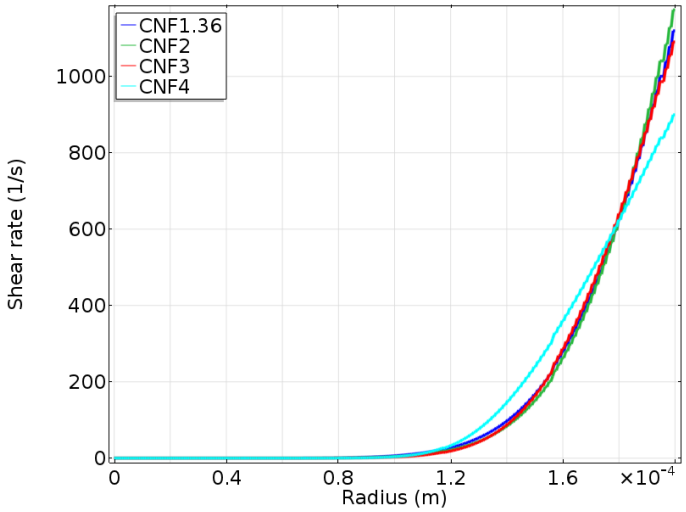

Figure 33: *Effect of concentration of fibrils on flow properties along the radius of the capillary tube for study [22]:* ***(a)*** *velocity profiles* ***(b)*** *shear rate profiles.*

(a)

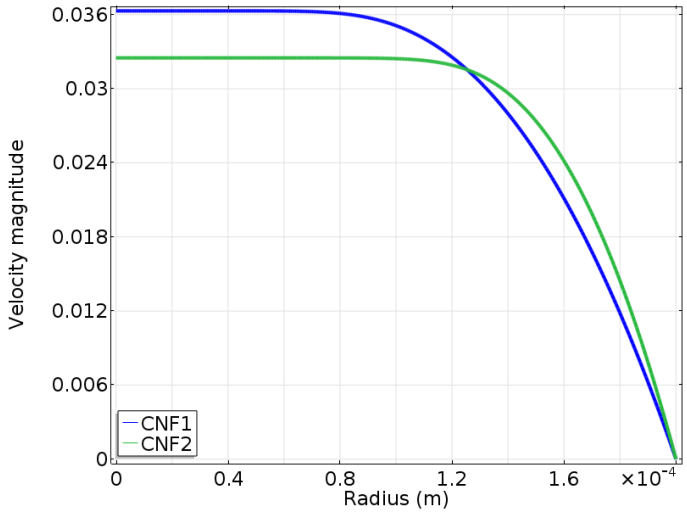

(b)

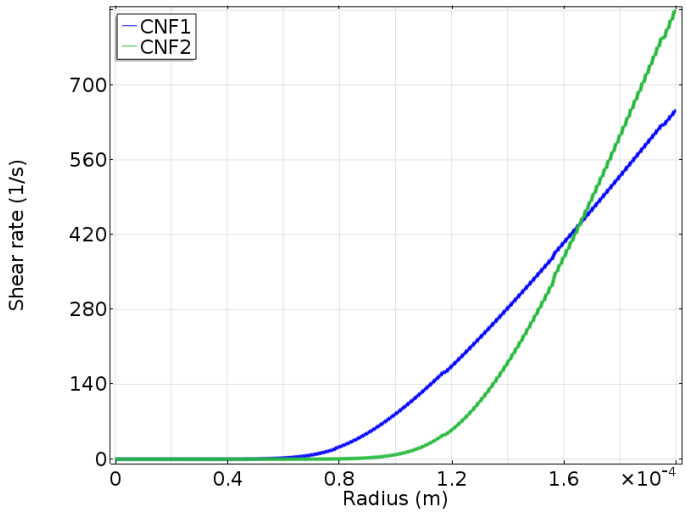

***Figure 34**: Effect of the concentration of the fibrils on the flow properties along the radius of the capillary tube from study [21]: **(a)** velocity profiles **(b)** shear rate profiles.*

Effect of Diameters

(a)

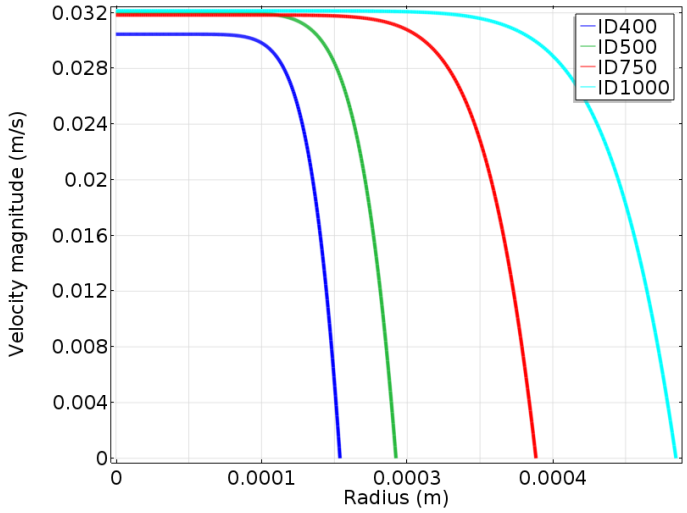

(b)

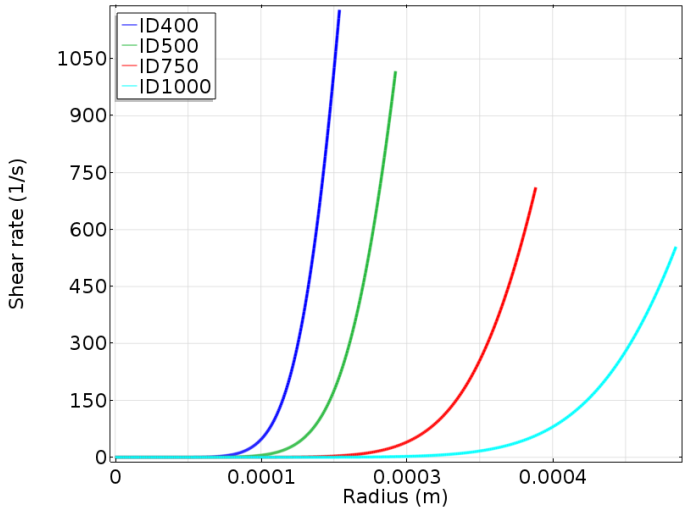

Figure 35: *Effect of the diameters of the capillary tube on the flow properties along the radius of the capillary tube:* ***(a)*** *velocity profiles* ***(b)*** *shear rate profiles.*

Effect of Flow Rate

(a)

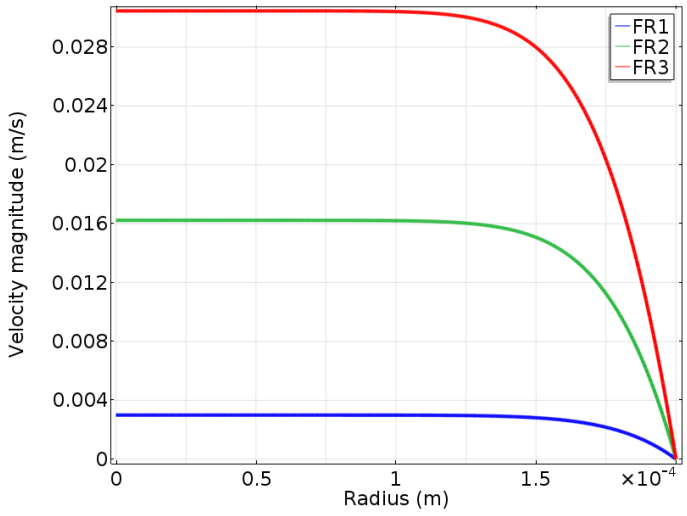

(b)

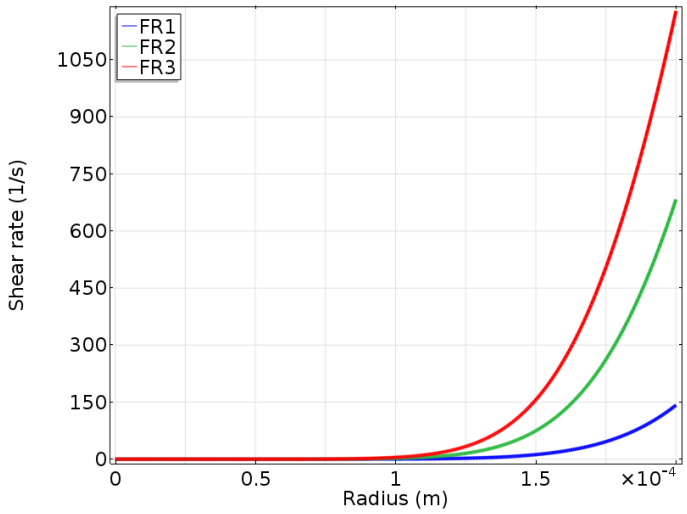

Figure 36: *Effect of the linear flow rate inside the capillary tube on the flow properties along the radius of the capillary tube:* ***(a)*** *velocity profiles* ***(b)*** *shear rate profiles.*

APPENDIX 2 – INLET PRESSURE MAGNITUDES

All the simulations are carried out by using pressure magnitude at inlet. Flow rates at inlet were known for the present study but corresponding pressure magnitudes were not available. Pressure values are obtained from the simulations carried out by describing the flow rates at inlet. Pressure magnitudes corresponding to the flow rates for each case are listed in **Table 2**.

TABLE 2: INLET PRESSURE VALUES CORRESPONDING TO THE GIVEN FLOW RATES

Case 1 (Highest flow rate, varying concentration, Diameter ID 400		
Concentration of CNF	Flow rate inlet [ml/min]	Pressure Inlet [Pa]
CNF1.36	0.183	31960
CNF2	0.183	73380
CNF3	0.183	187900
CNF4	0.183	307300
Case 2 (Highest flow rate, varying diameters, CNF2)		
Diameters	Flow rate inlet [ml/min]	Pressure Inlet [Pa]
ID400	0.183	75260
ID500	0.3	59700
ID750	0.666	38900
ID1000	1.183	28960

REFERENCE

[1] M. Vehviläinen, "Wet Spinning of Cellulosic Fibers from Water Based Solution Prepared from Enzyme Treated Pulp" , Tampere University of Technology, 2015.

[2] Z. K. Nagy *et al*, "Comparison of Electrospun and Extruded Soluplus-Based Solid Dosage Forms of Improved Dissolution", *Journal of Pharmaceutical Sciences,* vol. 101, pp. 322-332, 2011.

[3] S. Youssefian and N. Rahbar, "Molecular Origin of Strength and Stiffness in Bamboo Fibrils", *Scientific Reports,* vol. 5, 06/08, 2015.

[4] G. Josefsson, F. Berthold and E. K. Gamstedt, "Stiffness contribution of cellulose nanofibrils to composite materials", *International Journal of Solids and Structures,* vol. 51, pp. 945-953, 2014.

[5] M. Jonoobi, A. P. Mathew and K. Oksman, "Producing low-cost cellulose nanofiber from sludge as new source of raw materials", *Industrial Crops and Products,* vol. 40, pp. 232-238, 2012.

[6] I. Sakurada, Y. Nukushina and T. Ito, "Experimental determination of the elastic modulus of crystalline regions in oriented polymers", *Journal of Polymer Science,* vol. 57, pp. 651-660, 1962.

[7] H. Savastano Jr., P. G. Warden and R. S. P. Coutts, "Microstructure and mechanical properties of waste fiber–cement composites", *Cement and Concrete Composites,* vol. 27, pp. 583–592, 2005.

[8] G. H. D. Tonoli, H. Savasanto Jr., "Eucalyptus pulp fibres as alternative reinforcement to engineered cement-based composites", *Industrial Crops and Products,* vol. 31, pp. 225–232, 2010.

[9] F. de A. Silva, R. D. T. Filho, "Physical and mechanical properties of durable sisal fiber-cement composites", *Construction and Building Materials,* vol. 24, pp. 777-785, 2010.

[10] H. Savastano Jr., P. G. Warden and R. S. P. Coutts, "Ground iron blast furnace slag as a matrix for cellulose-cement materials", *Cement and Concrete Composites,* vol. 23, pp. 389-397, 2001.

[11] J. R. Rapoport, "Cast-in-Place Cellulose Fiber-Reinforced Cement Paste, Mortar, and Concrete", *Materials Journal,* vol. 102, pp. 299-306, 2005.

[12] N. K. Vasiliev and A. D. C. Pronk, "Ice composites as construction materials in projects of ice structures", in *Proceedings of the 23rd International Conference on Port and Ocean Engineering Under Arctic Conditions,* Trondheim, Norway, 2015.

[13] S. J. Eichron, "Review: Currrent international research into cellulose nanofibers and nanocomposites", *Journals of Master Science,* vol. 45, pp. 1-33, 2009.

[14] D. H. Page and F. elHosseiny, "The mechanical properties of single woodfibres. part vi. fibril angle and the shape of the stress-strain curve", *Journal of Pulp and Paper Science,* vol. 9, pp. 99-100, 1983.

[15] S. Iwamoto, A. Isogai and T. Iwata, "Structure and Mechanical Properties of Wet-Spun Fibers Made from Natural Cellulose Nanofibers", *Biomacromolecules,* vol. 12, pp. 831–836, 2011.

[16] P. Mohammadi, "Stiff and tough cellulose nanocomposite fibers through a biomimetic spinning approach", unpublished.

[17] D. Klemm, "Nanocellulose Materials - Different Cellulose, Different Functionality", *Macromolecules Symposia,* vol. 280, pp. 60-70, 2009.

[18] K. M. O. Håkansson, "Hydrodynamic alignment and assembly of nanofibrils resulting in strong cellulose filaments", *Nature Communications,* vol. 5, pp. 4018, 2014.

[19] M. M. Hamedi, "Highly Conducting, Strong Nanocomposites Based on Nanocellulose-Assisted Aqueous Dispersions of Single-Wall Carbon Nanotubes. ", *ACS Nano,* vol. 8, pp. 2467-2476, 2014.

[20] J. G. Torres-rendon, "Mechanical Performance of Macrofibers of Cellulose and Chitin Nanofibrils Aligned by Wet-Stretching: A Critical Comparison", *Biomacromolecules,* vol. 15, pp. 2709-2717, 2014.

[21] M. J. Lundahl, "Strength and Water Interactions of Cellulose I Filaments Wet-Spun from Cellulose Nanofibril Hydrogels", *Scientific Reports,* vol. 6, pp. 30695, 2016.

[22] Y. Shen, "High Velocity Dry Spinning of Nanofibrillated Cellulose (CNF) Filaments on an Adhesion Controlled Surface with Low Friction", *Cellulose,* vol. 23, pp. 3393-3398, 2016.

[23] R. Xiong, "Preparation and Properties of Fibers Produced from a Cellulose/complex PA Solvent System Precipitating in Diverse Coagulants", *Fibers Polymers,* vol. 14, pp. 926-934, 2013.

[24] A. Bendahou, H. Kaddami and A. Dufresne, "Investigation on the effect of cellulosic nanoparticles' morphology on the properties of natural rubber based nanocomposites", *European Polymer Journal,* vol. 46, pp. 609-620, 2010.

[25] Y. Habibi and M. R. Vignon, "Optimization of cellouronic acid synthesis by TEMPO-mediated oxidation of cellulose III from sugar beet pulp", *Cellulose,* vol. 15, pp. 177-185, 2008.

[26] A. Alemdar and M. Sain, "Isolation and characterization of nanofibers from agricultural residues - Wheat straw and soy hulls", *Bioresource Technology.,* vol. 99, pp. 1664-1671, 2008.

[27] W. F. Holzer, *Cellulose and Cellulose Derivatives.* NEW YORK: INTERSCIENCE PUBLISHERS, INC., 1954.

[28] J. Gullichsen and H. Paulapuro, *Papermaking Science and Technology, Book 6A. Chemical Pulping.* Jyväskylä: Fapet Oy, 2000.

[29] M. Pääkko, "Enzymatic Hydrolysis Combined with Mechanical Shearing and High-Pressure Homogenization for Nanoscale Cellulose Fibrils and Strong Gels", *Biomacromolecules,* vol. 8, pp. 1934-1941, 2007.

[30] K. Missoum, M. N. Belgacem and J. Bras, "Nanofibrillated Cellulose Surface Modification: A Review", *Materials,* vol. 6, pp. 1745-1766, 2013.

[31] T. Saito, "Cellulose Nanofibers Prepared by TEMPO-Mediated Oxidation of Native Cellulose", *Biomacromolecules,* vol. 8, pp. 2485-2491, 2007.

[32] N. K. Mathur, "Rheology of hydrocolloidals", in *Industrial Galactomannan Polysaccharides* Anonymous New York: CRC Press, 2011, pp. 41–48.

[33] R. Gavillon and T. Budtova, "Aerocellulose: new highly porous cellulose prepared from cellulose-NaOH aqueous solutions", *Biomacromolecules,* vol. 9, pp. 269-77, 2008.

[34] E. Lasseuguette, D. Roux and Y. Nishiyama, "Rheological properties of microfibrillar suspension of TEMPO-oxidized pulp", *Cellulose,* vol. 15, pp. 425-433, 2008.

[35] A. Puisto, "Modelling of rheology of CNF suspensions", *Nordic Pulp and Paper Research,* vol. 27, pp. 277-281, 2012.

[36] M. von Smoluchowski, "Versuch einer mathematischen Theorie der Koagulationskinetik kolloider Lösungen", *Zeitschrift Für Physikalische Chemie,* vol. 92, pp. 129, 1917.

[37] M. U. Bäbler, "A collision efficiency model for flow-induced coagulation of fractal aggregates", *AIChE Journal,* vol. 54, pp. 1748-1760, 2008.

[38] H. Mertaniemi, "Human Stem Cell Decorated Nanocellulose Threads for Biomedical Applications", *Biomaterials,* vol. 82, pp. 208-220, 2016.

[39] C. Green, "Dimensional properties of paper structures", *Industrial & Engineering Chemistry Product Research and Development,* vol. 20, pp. 151-158, 1981.

[40] M. N. Vyakamam and L. T. Drzal, "A new process for aligning fibers in composites", *Plastics Engineering,* vol. 53, pp. 35-37, 1997.

[41] T. Itoh, S. Masuda and F. Gomi, "Electrostatic orientation of ceramic short fibers in liquid", *J. Electrostatics,* vol. 32, pp. 71-89, 1994.

[42] B. Nordstrom and B. Norman, "Influence of sheet anisotropy, formation, toughness and tensile stiffness of reduced feed area to a headbox nozzle", *Nordic Pulp and Paper Research,* vol. 9, pp. 53–59, 1994.

[43] J. A. Olson, P. J. Krochak1 and D. M. Martinez, "The orientation of semidilute rigid fiber suspensions in a linearly contracting channel", *Physics of Fluids,* vol. 20, 2008.

[44] G. B. Jeffery, "The Motion of Ellipsoidal Particles Immersed in a Viscous Fluid", *Proceedings of the Royal Society of London A: Mathematical, Physical Engineering Science,* vol. 102, pp. 161, 1922.

[45] S. G. Mason, C. E. Chaffey and H. Brenner, "Particle motions in sheared suspensions", *Rheologica Acta,* vol. 4, pp. 64-72, 1965.

[46] K. Håkkanason, "Orientation Elongated, Macro and Nano-Sized Particles in Macroscopic" , KTH Royal Institute of Technology, Stockholm, 2014.

[47] F. Truckenmuller and H. G. Fritz, "Injection molding of long fiber-reinforced thermoplastics: a comparison of extruded and pultruded materials with direct addition of roving strands", *Polymer Engineering and Science,* vol. 31, pp. 1316 - 1329, 1991.

[48] E. D. Kragness, M. F. Amateau and G. L. Messing, "Processing and Characterization of Laminated SiC Whisker Reinforced Al2O3", *Journal of Composite Materials,* vol. 25, pp. 416-432, 1991.

[49] R. A. J. Sambell, D. H. Bowen and D. C. Phillips, "Carbon fibre composites with ceramic and glass matrices", *Journal of Materials Science,* vol. 7, pp. 663-675, 1972.

[50] K. Lee, "On the use of nanocellulose as reinforcement in polymer matrix composites", *Composites Science and Technology.,* vol. 105, pp. 15-27, 2014.

[51] D. E. Dingle, "Aligned, discontinuous carbon-fibre composites", in *International Conference on Carbon Fibres; their Place in Modern Technology,* Plastics Institute, London, 1974, pp. 78.

[52] D. C. Guell and A. L. Graham, "Improved Mechanical Properties in Hydrodynamically Aligned, Short-Fiber Composite Materials", *Journal of Composite Materials,* vol. 30, pp. 2-12, 1996.

[53] D. Guell and A. Bénard, "Flow-induced alignment in composite materials: Current applications and future prospects", in *Flow-Induced Alignment in Composite Material* Cambridge: Woodhead Publishing, 1997, pp. 1-42.

[54] C. Y. Kim, "The mechanical properties of single wood pulp fibers. III. The effect of drying stress on strength", *Journal of Applied Polymer Science,* vol. 19, pp. 1549-1562, 1975.

[55] M. J. Lundahl *et al*, "Spinning of Cellulose Nanofibrils into Filaments: A Review", *Industrial & Engineering Chemistry Research,* vol. 56, pp. 8-19, 2017.

[56] J. C. Malzahn and J. M. Schultz, "Tension-tension and compression-compression fatigue behavior of an injection-molded short-glass-fiber/poly(ethylene terephthalate) composite", *Composites Science and Technology,* vol. 27, pp. 253-289, 1986.

[57] E. J. Tozzi, "Effect of fiber length, flow rate, and concentration on velocity profiles of cellulosic fiber suspensions", *Acta Mechanica,* vol. 224, pp. 2301-2310, 2013.

[58] F. M. White, Ed., *Fluid Mechanics.* New York: McGraw-Hill Education, 2010.

[59] G. Barr, "A Monograph of Viscometry", 1931.

[60] R. P. Chhabra and J. F. Richardson, *Non-Newtonian Flow in the Process Industries.* Oxford: Butterworth Heinemann, 1999.

[61] M. Chatzimina, "Cessation of annular Poiseuille flows of Bingham plastics", *Journal of Non-Newtonian Fluid Mechanics,* vol. 142, pp. 135-142, /3/16/, 2007.

[62] O. Gonzalez and A. M. Stuart, "Isothermal fluid mechanics", in *A First Course in Continuum Mechanics* London: Cambridge University Press, 2008, pp. 221-270.

[63] M. A. Rao, *Rheology of Fluid, Semisolid, and Solid Foods.* New York: Springer Science+Business Media, 2014.

[64] Anonymous, "The Finite Element Method", [Online]. Available: https://www.comsol.de/multiphysics/finite-element-method. [Accessed: 23- Jan- 2017].

[65] Anonymous, "Viscosity Model (Thermoplastic Only)" [Online]. Available: http://support.moldex3d.com/r13/moldex3d/module-introduction/standard-injection molding. [Accessed: 20- Feb- 2017]

[66] W. Frei, "The Finite Element Method", [Online]. Available: https://www.comsol.com/blogs/meshing-your-geometry-various-element-types. [Accessed: 23- Jan- 2017].